Redox Biology 52 (2022) 102287

Contents lists available at ScienceDirect

Redox Biology

journal homepage: www.elsevier.com/locate/redox

The amyloid peptide β disrupts intercellular junctions and increases endothelial permeability in a NADPH oxidase 1-dependent manner

Anuradha Tarafdar [a,b,1], Nina Wolska [c,1], Christoph Krisp [d], Hartmut Schlüter [d], Giordano Pula [c,e,*]

[a] Cancer Research UK Therapeutic Discovery Laboratory, Babraham Research Campus, Cambridge, UK
[b] Institute of Biomedical & Clinical Science, University of Exeter Medical School (UEMS), Exeter, UK
[c] Institute for Clinical Chemistry and Laboratory Medicine, University Medical Center Eppendorf (UKE), Hamburg, Germany
[d] Section of Mass Spectrometry and Proteomics - Institute for Clinical Chemistry and Laboratory Medicine, University Medical Center Eppendorf (UKE), Hamburg, Germany
[e] Centre for Atherothrombosis and Metabolic Disease (CAM), Hull and York Medical School (HYMS), Hull, UK

ARTICLE INFO

Keywords:
Alzheimer
Endothelial
NADPH oxidase
Oxidative stress
Permeability
Neuroinflammation

ABSTRACT

Alzheimer's disease is the most common form of dementia and is associated with the accumulation of amyloid peptide β in the brain parenchyma. Vascular damage and microvascular thrombosis contribute to the neuronal degeneration and the loss of brain function typical of this disease. In this study, we utilised a murine model of Alzheimer's disease to evaluate the neurovascular effects of this disease. Upon detection of an increase in the phosphorylation of the endothelial surface receptor VE-cadherin, we focused our attention on endothelial cells and utilised two types of human endothelial cells cultured *in vitro*: 1) human umbilical vein endothelial cells (HUVECs) and 2) human brain microvascular endothelial cells (hBMECs). Using an electrical current impedance system (ECIS) and FITC-albumin permeability assays, we discovered that the treatment of human endothelial cells with amyloid peptide β causes a loss in their barrier function, which is oxidative stress-dependent and similarly to our observation in mouse brain associates with VE-cadherin phosphorylation. The activation of the superoxide anion-generating enzyme NADPH oxidase 1 is responsible for the oxidative stress that leads to the disruption of barrier function in human endothelial cells *in vitro*. In summary, we have identified a novel molecular mechanism explaining how the accumulation of amyloid peptide β in the brain parenchyma may induce the loss of neurovascular barrier function, which has been observed in patients. Neurovascular leakiness plays an important role in brain inflammation and neuronal degeneration driving the progression of the Alzheimer's disease. Therefore, this study provides a novel and promising target for the development of a pharmacological treatment to protect neurovascular function and reduce the progression of the neurodegeneration in Alzheimer's patients.

1. Introduction

Dementia is one the most common ageing-related pathologies and it is used as an umbrella term to define a cluster of symptoms involving progressive impairment in brain cognitive functions that can eventually lead to decreased quality of life, physical disability and

Abbreviations: AJs, Adherens junctions; AD, Alzheimer's disease; APP, Amyloid precursor protein; BBB, Blood brain barrier; COX2, Cyclooxygenase 2; ECIS, Electrical current impedance system; EPR, Electron paramagnetic resonance; FITC, Fluorescein isothiocyanate; HO-1, Heme oxygenase-1; HUVECs, Human umbilical vein endothelial cells; hBMECs, Human brain microvascular endothelial cells; IFN-γ, Interferon γ; IL-1α, Interleukin-1α; IP-10, IFN-γ-induced protein 10; NADPH, Nicotinamide adenine dinucleotide phosphate; Nrf-2, Nuclear factor erythroid 2–related factor 2; PS1, Presenilin 1; ROS, Reactive oxygen species; RAGE, Receptor for advanced glycation end products; RANTES, Regulated upon activation, normal T cell expressed and presumably secreted; SEM, Standard error; siRNA, Small interfering RNA; TJs, Tight junctions; TNF α, Tumour necrosis factor α; VCAM-1, Vascular cell adhesion molecule 1.

* Corresponding author. Institute for Clinical Chemistry and Laboratory Medicine, University Medical Center Eppendorf (UKE), Martinistrasse 52, D-20246, Hamburg, Germany.
E-mail address: g.pula@uke.de (G. Pula).
[1] authors contributed equally.

https://doi.org/10.1016/j.redox.2022.102287
Received 8 December 2021; Received in revised form 12 March 2022; Accepted 12 March 2022
Available online 25 March 2022

institutionalization [1]. There are an estimated 46.8 million people living with dementia worldwide and the numbers of patients will double every 20 years, rising to 115.4 million in 2050. The most dominant form of dementia is the Alzheimer's disease (AD), which is responsible for 60–80% of dementia cases [2]. AD is a multifactorial and progressive neurodegenerative disease of the brain that was first described by the German psychiatrist Alois Alzheimer in 1906 [3]. AD is associated with the deposition of plaques formed by amyloid peptides β and the accumulation of hyperphosphorylated tau proteins in the brain. In turn, this causes inflammation, blood flow impairment (or hypoperfusion), and neuronal death, ultimately resulting in the progressive cognitive deterioration [4]. Cerebral blood hypoperfusion is particularly important in the development of AD, as it contributes to accumulation of toxic metabolites, ineffective clearance of amyloid peptides and reduced oxygenation of the brain [5,6]. The study of the effect of AD and especially amyloid peptide β accumulation on neurovascular cells is a growing and promising research area for the discovery of novel ways to treat this disease and control the dementia pandemic.

In AD brain, substantial morphological and functional cerebrovascular abnormalities are observed, including microvasculature irregularities and atrophy, basement membrane disruption and deposition of heparin sulphate proteoglycans, collagen IV and laminin, decreased cerebrovascular network density, endothelial cell alteration i.e. increased pinocytosis, decreased levels of mitochondria and detection of elevated endothelial cell markers VCAM-1 and E-selectin [7–10]. Cerebrovascular abnormalities associated with AD can result in hypoperfusion, hypoxia, inflammation and disruption of the blood brain barrier (BBB). These vascular alterations are referred to as cerebral amyloid angiopathy or CAA, which is associated with ischemic lesions, micro- and macro-haemorrhages, and impaired cerebral blood flow. Ultimately, impaired blood flow and resulting ischemia exacerbate neurodegeneration and accelerate the progression of AD [11–13]. In addition, intimal inflammation and endothelial damage are likely to contribute to platelet stimulation in AD patients [14]. Several studies indicated elevated levels of inflammatory mediators in AD cerebral microcirculation, where endothelial cells overexpress cyclooxygenase 2 (COX2) [15], adhesion molecules (MCP-1, ICAM-1, CAP37), and inflammatory and stress markers, such as TNFα, TGF-β, interleukins (IL-1β, IL-6, IL-8) and metalloproteinases (MMPs) [16–18]. The inflammatory proteins overexpressed in the AD cerebrovasculature are likely to have toxic effects on neurons, which could represent an important link between vascular inflammation and neuronal loss in AD [19].

Recent studies suggested a causative link between the accumulation of amyloid peptide β in the brain and the loss of barrier function of endothelial cells [20]. Oxidative stress has been shown to link amyloid peptide β accumulation and neurovascular damage [21,22]. NADPH oxidases (NOXs) are key sources of ROS in neurovascular cells [23] and have been shown to play an important role in neurodegenerative diseases [24]. Although previous studies suggested a role for NOX2 in the amyloid β-dependent changes in cerebrovascular permeability [25], in this study we show for the first time a key role for NOX1 in the loss of barrier function and motility by endothelial cells exposed to amyloid peptide β. The amyloid β-dependent increase in endothelial monolayer permeability was associated with the phosphorylation of VE-cadherin, an event shown to cause the loosening of adherens junctions (AJs) and the inhibition of the endothelial cell barrier function [26,27]. In our experiments, VE-cadherin was also hyperphosphorylated in the brain of the AD model 3xTG-AD [28]. Overall, this study indicates a prominent role of NOX1 in the amyloid β-dependent impairment of the normal endothelial function in AD brains. NOX1 is therefore a promising target for the development of neuroprotective agents in the fight against AD.

2. Material and methods

2.1. 3xTG-AD mice maintenance, perfusion fixation and brain sectioning

All animal experiments complied with the ARRIVE guidelines. Mouse maintenance and sacrifice was approved by the local ethics committee (University of Exeter) and Home Office Project licence 3003348. Triple mutant mice were utilised as a model of AD (APP Swedish, MAPT P301L, and PSEN1 M146V) [28]. B6129SF2 wild-type mice were used as controls. Intra-cardiac perfusions with 4% paraformaldehyde were performed on 6 and 12 month old female mice as previously described [29]. The brains were collected in 4% paraformaldehyde and transferred to PBS before embedding them in paraffin for sectioning (10 μm thickness).

2.2. Differential quantitative proteomics of mouse hippocampus

The hippocampus was excised from paraformaldehyde-fixed mouse brain sections (100 μm thickness) and lysed in 1% w/v sodium deoxycholate - 100 mM triethyl ammonium bicarbonate buffer. After boiling for 1 h at 95 °C for antigen retrieval, samples were sonicated and reduced in the presence of 10 mM dithiotreitol. Samples were alkylated in presence of 20 mM iodoacetamide and the tryptic digestion of 20 μg was performed at a 50:1 protein to enzyme ratio overnight. Samples were resuspended in 0.1% w/v formic acid and chromatographic separation was achieved on a Dionex Ultimate 3000 UPLC system (Thermo Fisher Scientific) with a two-buffer system (buffer A: 0.1% w/v formic acid in water, buffer B: 0.1% w/v formic acid in acetonitrile). Peptides were separated using a 60 min gradient with increasing ACN concentration from 2% to 30% v/v. The eluting peptides were analysed on a quadrupole orbitrap mass spectrometer (QExactive, Thermo Fisher Scientific). The QExactive was used to analyze the top 12 most intense ions per precursor scan (1 × 10 [6] ions, 70,000 Resolution, 120 ms fill time) and were analysed by MS/MS in the orbitrap (HCD at 25 normalized collision energy, 17,500 resolution, 1 × 10 [5] ions, 50 ms fill time) in a range of 400–1300 *m/z*. Acquired LC-MS/MS data were searched against the reviewed mouse protein data base Uniprot (October 2020, 17,053 protein entries, EMBL) using the Sequest algorithm integrated in the Proteome Discoverer software version 2.4 (Thermo Fisher Scientific). Only peptide with a high confidence (false discovery rate <1% using a decoy data base approach) were accepted as identified. Peptide precursor area under the curve values were summed to protein areas and used for quantitative analysis. Protein areas were imported into Perseus software version 1.5.8 for statistical analysis. Proteins with a T-test p values < 0.05 and expression difference±15% were considered differentially expressed. Pathway analysis was performed using the STRING software (https://string-db.org/, version 11.5, by Peer Bork, Lars Juhl Jensen, and Christian von Mering, © String Consortium 2022) and the Reactome Pathway Database (https://reactome.org/, © Reactome 2022).

2.3. Mouse hippocampus imaging

Brain sections were deparaffinized (3x wash xylene for 15 min each, 1x wash 50% xylene/50% ethanol, 1x wash ethanol, 1x wash methanol for 3 min each, 2x of 95% ethanol for 10 min each, 2x wash in ddH_2O 5 min each), then heat-induced epitope retrieval was performed (10 mM sodium citrate pH 6, 10 min, 90 °C, then 2x wash in tap water). Afterwards the sections were stained with Thioflavin S (1% w/v solution in 50% ethanol, T1892, Sigma-Aldrich, St Louis, US) for 15 min, then destained with 50% ethanol for 5 min and washed extensively with PBS. For immunofluorescence staining, sections were blocked with 3% v/v donkey serum in PBS-TritonX-100 (0.5% v/v), then stained with antibodies against amyloid peptide β (BioLegend #803001, 1:100), VE-cadherin (R&D Systems, #AF1002, 1:100), and phosphorylated VE-cadherin (Abcam, #ab49785, 1:50) overnight at 4 °C, then washed 3x PBS-TritonX-100 (0.5% v/v), stained with secondary antibodies and

DAPI, and the autofluorescence was quenched with 0.1% w/v solution of Sudan Black. Coverslips were mounted with Fluoromount mounting medium. The imaging was performed with the Leica TCS SP5 confocal microscope (Leica, Wetzlar, Germany). Images were analysed using the FIJI software [30] and staining intensity is expressed as mean intensity ratio (phospho-VE-cadherin vs total VE-cadherin).

2.4. Endothelial cell culture

Mycoplasma free Human Umbilical Vein Endothelial Cells (HUVECs) were purchased from Lonza and were routinely cultured in EGM-2™ (Endothelial Cell Growth Medium-2) supplemented with SingleQuots™ Supplements. Human Brain Microvascular Endothelial Cells (hBMECs) were purchased from Science Cell Research Laboratories (Carlsbad, US) and were cultured in Endothelial Cell Medium (ECM) supplemented with Endothelial Cell Growth Supplement (ECGS), Foetal Bovine Serum (FBS) and penicillin/streptomycin solution were all from Science Cell Research Laboratories. Incubation with amyloid peptide β 1–42 (DAEFRHDSGYEVHHQKLVFFAEDVGSNKGAIIGLMVGGVVIA) or scrambled control (DEFAKNIGHHDGVAVHMYKGRQVEFIGSIALVFDEVGSAGLV) was performed with a maximal DMSO concentration of 0.2% v/v. For gene silencing with siRNA, HUVECs were transfected with NOX1 (#sc-43939), NOX2 (#sc-35503), NOX4 (#sc-41586), NOX5 (#sc-45486) or scrambled control (#sc-37007) siRNAs (Santa Cruz Biotechnology) as per manufacturer's instructions. In brief, the siRNAs were diluted to 100 nM in transfection medium (#sc-36868; Santa Cruz Biotechnology) containing transfection reagent (#sc-29528; Santa Cruz Biotechnology), incubated for 45 min at room temperature, and then further diluted to 20 nM in transfection medium. The cells were incubated with the transfection medium for 5 h at 37 °C, after which growth medium containing normal concentrations of serum and growth factors was added. Experiments were performed 48 h after transfection.

2.5. Quantitative reverse transcription PCR (RT-qPCR) analysis

2 × 10 [5] HUVECs were cultured in Nunc™ cell culture treated 6-well plates. The cells were treated with 25 μM Aβ1-42, SCR peptide or DMSO as vehicle control for 8 h or 24 h. Where indicated, cells were pre-treated with 10 μM VAS2870 before treatment with Aβ1-42 or SCR peptide. For RT-PCR, total RNA was extracted using TRIzol™ reagent (Thermo Fisher Scientific) according to manufacturer's instructions. 1 μg of RNA was reverse transcribed to make cDNA using the Applied Biosystems™ High-Capacity cDNA Reverse Transcription Kit (Thermo Fisher Scientific) according to manufacturer's instructions. Gene specific amplification for was performed on QuantStudio™ 7 Flex Real-Time PCR System and quantified using Power SYBR Green PCR Master Mix (Thermo Fisher Scientific). IL-1β, VCAM, RAGE, HMOX and NRF2 primers were purchased from Sigma, while NOX1, NOX2 NOX4 and NOX5 primers were designed (Nox1 Forward TTGAAAGGTTGGGTTTAGCTG (21); Nox1 Reverse AAATGGAACCCTTGGAGCA (19); Nox2 Forward AAGAGAAACT CCTCTGCTGTGAA (23); Nox2 Reverse CGCACTGGAACCCCTGAGAAAGG (23); Nox4 Forward: CAGATGTTGGGGCTAGGATT (20) Nox4 Reverse: AGAAGTTGAGGGC ATTCACC (20); Nox5 Forward CCAGTGCCTCAACTTCGACT (20); Nox5 Reverse GCCCATAAGCT GGTGGAACT (20)). The $2^{-\Delta\Delta CT}$ method was used to calculate relative expression levels for each gene with GAPDH and actin as endogenous controls as previously described [31].

2.6. Immunoblotting, ELISA and immunocytochemistry of endothelial cells

2 × 10 [5] HUVECs were cultured in Nunc™ cell culture treated 6-well plates. The cells were treated with 25 μM Aβ1-42, SCR peptide or DMSO as vehicle control for 24 h. To harvest proteins, the cells were lysed in radioimmunoprecipitation assay (RIPA) buffer in the presence of protease and protein phosphatase inhibitor cocktails 2 and 3 (Merck-Sigma). Sodium dodecyl sulphate polyacrylamide gel electrophoresis (SDS-PAGE) was used to separate proteins as described previously [32]. Antibodies for phospho-VE cadherin (Y658) (Invitrogen, #44-1144G) and total VE-cadherin (Santa Cruz, #sc-9989) were purchased from commercial suppliers. The NOX1 antibody was from Novus Biologicals (#NBP1-31546). Actin from Merck-Sigma was used as loading control. Immunoblot densitometry was performed using Image studio Version 5.2 (LI-COR Biosciences). For ELISA, the culture medium from HUVECs treated as described above was analysed using a commercial inflammation ELISA kit following manufacturer instructions (Signosis, #EA-1031). For HUVEC immunocytochemistry, cells were cultured on cell culture-compatible coverslips for 48 h to reach 95% confluence. Following fixation in 4% w/v paraformaldehyde, cells were stained with anti-VE-cadherin antibody (#ab33168 from Abcam), fluorescein isothiocyanate (FITC)-labelled secondary antibodies and 4′, 6-diamidino-2-phenylindole (DAPI). The imaging was performed with the Leica TCS SP5 confocal microscope (Leica, Germany) and densitometry was performed using the FIJI software [30].

2.7. Apoptosis assay by flow cytometry

After incubation, cells were harvested with the gentle dissociating buffer TrypLE®, pelleted by centrifugation, washed with PBS, and resuspended in PBS. Cell suspensions were stained with Annexin V/FITC + propidium iodide (PI) according to the manufacturer's instructions (Thermo Fisher Scientifics, #88–8005). After 15 min of incubation in the dark on ice, cells were centrifuged at 2000 rpm for 10 min, resuspended in PBS, and analysed using a FACSCanto II (BD Biosciences). Annexin V/PI scatter plots divided in quadrants were utilised to assess early apoptotic (Annexin V^+/PI^-), late apoptotic (Annexin V^+/PI^+) and necrotic (Annexin V^-/PI^+) cells.

2.8. Electron paramagnetic resonance (EPR)

1 × 10 [4] HUVEC or hBMECs were cultured in triplicate in Nunc™ cell culture treated 96-well plates for 24 h. Aβ1-42, scrambled control peptide DMSO or NOX inhibitors were added as indicated for 4 h 200 μM 1-hydroxy-3-methoxycarbonyl-2,2,5,5-tetramethylpyrrolidine (CMH), 5 μM diethyldithiocarbamate (DETC) and 25 μM deferoxamine were then added to the cultures for 45 min 50 μL of supernatant were transferred into the Hirschmann precision micropipettes and read using an e-scan (Noxygen, Germany), as previously described [33]. EPR spectra were recorded using the following EPR settings: centre field 3492.5 G, field sweep 60 G, modulation amplitude 2 G, sweep time 10 s, number of scans 10, microwave frequency 9.39 GHz, microwave power 20 mW, conversion time 327.68 ms, time constant 5242.88 ms. A calibration curve was obtained from standard $CM^{\bullet}$ diluted to concentrations of 0, 0.3, 1, 3, 10, and 30 μM and utilised to estimate the $CM^{\bullet}$ concentration in the samples as described in Supplementary Fig. 1. The CMH oxidation rate was obtained using the formula below:

$$\text{CMH oxidation rate} = [CM^{\bullet}] \times \text{Volume} / (\text{cell density} \times \text{Volume} \times \text{Time})$$

2.9. Electrical cell-substrate impedance sensing (ECIS)

The 8W1E PET arrays (AppliedBioPhysics) were electrically stabilised and collagen coated (#354233, Fisher Scientific) prior to the addition of cells as per manufacturer's protocol. 1 × 10 [5] cells/well were dispensed in 400 μl and allowed to settle in the wells at RT for 30 min before placing them in the incubator. Electrical impedance was measured at frequency 4000 Hz using a Model Z Theta from AppliedBioPhysics (NY, US), which estimates current leakage "between cells" and therefore informs about cell barrier function [34]. ECIS recordings reached a steady-state corresponding to the formation of a compact

endothelial cell monolayer within 24 h from cell seeding. The Aβ1-42, scrambled peptide or the drugs as indicated were prepared at 2X concentration in the culture medium and kept at 37 °C for 30 min before adding to the cells to minimize any unrelated impedance changes. 200 μl of media was removed very gently from the wells and replaced with 2X solutions containing treatment to reach the desired final concentration. In order to monitor the effect of Aβ1-42 on barrier function, the electrical impedance measurements were recorded for further 24 h (up to t = 48 h). Then, in order to study the effect Aβ1-42 on endothelial cell migration and reparative potential, electrical wounding was performed (time 1 s, current 1400 μA) and electrical impedance was measured for a further 24 h (up to t = 72 h).

2.10. FITC-albumin permeability assays

HUVECs or hBMECs were grown to confluence in the inserts of transwell plates (Costar #3413, pore size 0.4 μm). At the beginning of the experiments, the treatments were administered at the indicated concentrations (e.g. Aβ1-42, NoxA1 ds, etc.) and 1 mg/ml FITC-albumin (Thermo Scientifics, Albumin from Bovine Serum (BSA), FITC conjugate, cat. no. #A23015) was added. The filtration of FITC-albumin from the transwell insert to the bottom of the well was monitored over time (0–48 h) by fluorescence microplate reading (λ_{exc} = 490 nm) using a Spark 10 M microplate reader (Tecan, Männedorf, Switzerland).

2.11. Statistical analysis

Dual comparisons were analysed by non-parametric Mann-Whitney test. One-way ANOVA with Tukey post-test was used for multiple comparison tests after testing that data are normal and homoscedastic. For time courses (e.g. permeability assays), two-way ANOVA with Bonferroni post-test for different time points was utilised. The software

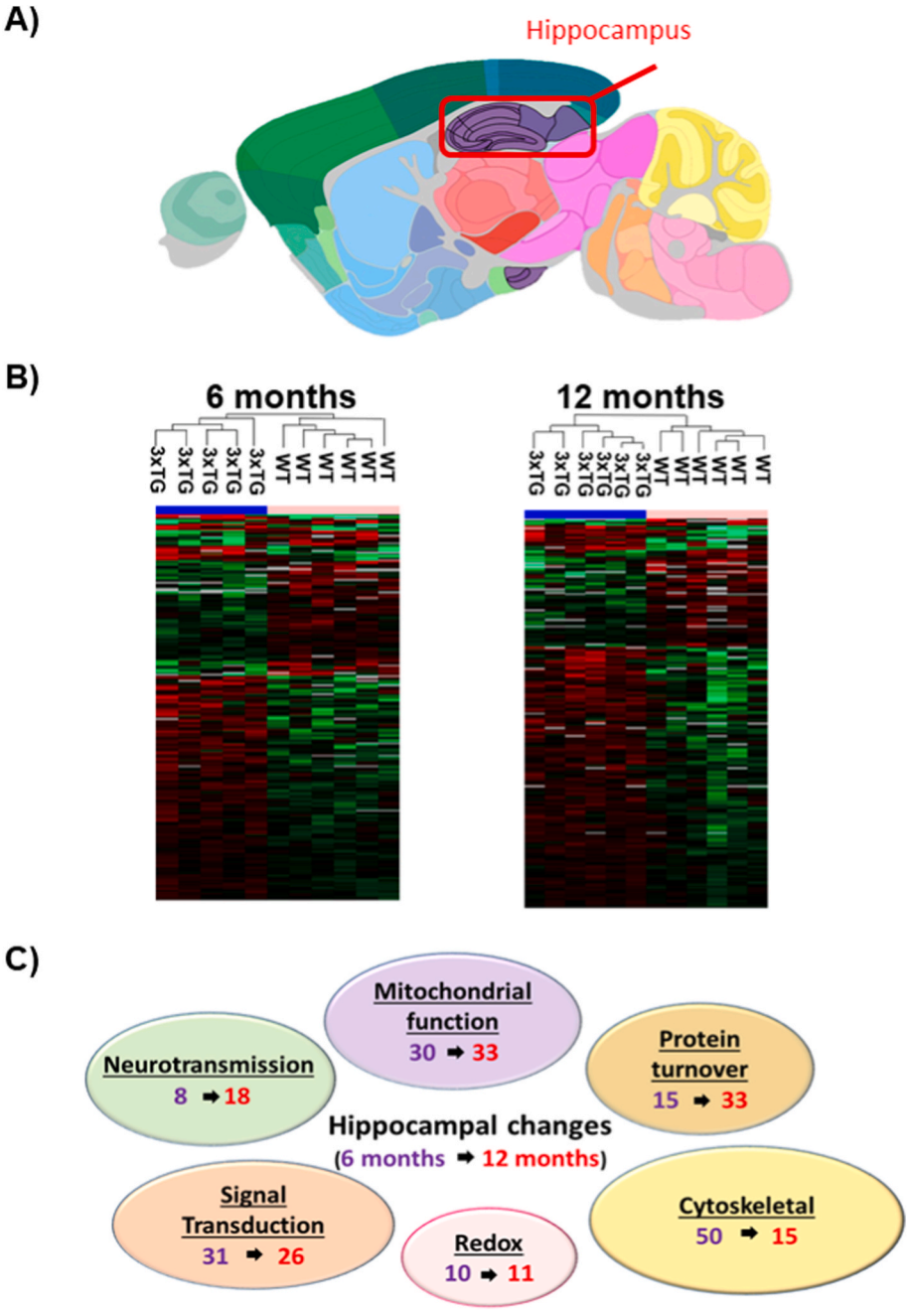

Fig. 1. Differences in the hippocampal proteome between 3xTG-AD and wild type mice at 6 and 12 months of age. The hippocampal proteome was obtained by selective sampling of the hippocampus region (sagittal view in A). The proteomics analysis at age 6 and 12 months is shown in B and C, respectively. Heat maps of the identified proteins (left panels) show clear and consistent clustering of 3xTG/AD mice versus wild type controls. Differentially expressed proteins are grouped by cellular function (right panels). Data were obtained from 6 animals per genotype and age. The number of proteins with expression levels statistically different between 3xTG/AD and wild type controls at age 6 months (purple) and 12 months (red) is indicated for each function group. The lists of proteins with quantitative data are shown in Tables 1–2 and Supplementary Tables 1–3.

package GraphPad Prism Version 8.1.0 for Windows 64 bit was used for all statistical analyses. Data normality and homoscedasticity were tested with Shapiro-Wilk and Bartlett's tests, respectively. Throughout the study, the results were expressed as the mean ± standard error (SEM). Differences were considered significant at P value < 0.05 (*), 0.01 (**) or 0.001 (***).

3. Results

3.1. Amyloid peptide beta deposition and gene expression changes in the hippocampus of 3xTG-AD mice

The AD model 3xTG-AD [28] and the wild type control B6129SF2 were maintained for 3, 6 and 12 months, which represent preclinical, early and advanced stages of the disease. The hippocampal region of the brain of the mice was analysed by LC-MS/MS based proteomics as described in the material and methods section (Fig. 1A). As shown in Supplementary Tables 1, 2,797 proteins were identified in the hippocampal sections. The proteomics analysis at age 6 and 12 months identified clear and consistent differences between 3xTG-AD and wild type mice (Fig. 1B and C, respectively). The comparison of 6 animals per group led to the identification of 224 and 228 differentially expressed proteins in the hippocampus of 3xTG-AD mice compared to wild type mice at 6 and 12 months of age, respectively. The complete list of proteins with differential expression is shown in Supplementary Tables 2 and 3, ordered by p value. The proteome analysis indicated statistically significant changes in the expression of proteins involved in important physiological processes, such as mitochondrial and cytoskeletal function, neurotransmission, intracellular signal transduction, protein synthesis and turnover, and redox homeostasis (Tables 1 and 2, for 6 and 12 months of age, respectively). Automated pathway analysis using the STRING software and the Reactome Pathway Database is shown in Fig. 2 and Supplementary Table 4. It highlighted significant changes in a number of metabolic pathways (citric acid pathway and amino acid pathways), membrane trafficking (including clathrin-mediated endocytosis), biological oxidations, and opioid signalling. At month 12, cell degradative pathways such as apoptosis and mitophagy were also significantly affected. The entire proteomics dataset is available in PRIDE (Project accession: PXD030300, Project DOI: 10.6019/PXD030300). Amyloid β deposits in the hippocampus of 3xTG-AD mice (versus B6129SF2 wild type) became evident at 6 and 12 months of age, as shown by Thioflavin-T staining (Fig. 3A). In addition, the hippocampal region of 3xTG-AD mice displayed significantly higher levels of VE-cadherin phosphorylation at the residue Tyr658 at 6 and 12 months of age compared to wild type controls (representative examples and densitometry analysis in Fig. 3B).

3.2. Amyloid peptide beta induces pro-inflammatory changes in endothelial cells in vitro

Cerebrovascular dysfunction has been suggested to cause extensive abnormalities of cerebral capillaries, which result in reduced cerebral blood flow in AD patients [35]. Therefore, we have investigated the effects of Aβ1-42 on endothelial cells *in vitro*. Quantitative reverse transcription PCR (RT-qPCR) was utilised to study the effect of Aβ1-42 on HUVECs. Four genes associated with pro/inflammatory responses of endothelial cells were found to be significantly increased by 8 h or 24 h of incubation with 25 μM of Aβ1-42 versus scrambled control peptide: receptor for advanced glycation end products (RAGE), vascular cell adhesion protein 1 also known as vascular cell adhesion molecule 1 (VCAM-1), Heme oxygenase-1 (HO-1) and nuclear factor erythroid 2–related factor 2 (Nrf2) (Fig. 4A). In addition, the secretion of pro-inflammatory cytokines tumour necrosis factor α (TNF α), interferon γ (IFN-γ), interleukin-1α (IL-1α), IFN-γ-induced protein 10 (IP-10) and "regulated upon activation, normal T cell expressed and presumably secreted" (RANTES) resulted increased by 24 h incubation with 25 μM of

Table 1
Selected differentially expressed proteins in the hippocampus of 3xTG-AD mice at 6 months of age divided by cellular function. The statistical significance of the difference was tested by Student T-test (n = 6).

Accession	Protein Name	Gene Name	P value
	Redox Homeostasis		
Q61696	Heat shock 70 kDa protein 1A	Hspa1a	0.000746776
O55125	Protein NipSnap homolog 1	Nipsnap1	0.003064161
Q9CY64	Biliverdin reductase A	Blvra	0.003573887
Q61165	Sodium/hydrogen exchanger 1	Slc9a1	0.008153903
P09671	Superoxide dismutase [Mn], mitochondrial	Sod2	0.019113985
Q9CR61	NADH dehydrogenase 1 beta subcomplex subunit 7	Ndufb7	0.027248613
Q8BMF3	NADP-dependent malic enzyme, mitochondrial	Me3	0.035158694
Q8C437	PEX5-related protein	Pex5l	0.036398034
Q9JJK2	LanC-like protein 2	Lancl2	0.043470887
Q9R0P3	S-formylglutathione hydrolase	Esd	0.04954031
	Neurotransmission		
Q9R0N7	Synaptotagmin-7	Syt7	0.001410352
O08599	Syntaxin-binding protein 1	Stxbp1	0.013051379
Q99NE5	Regulating synaptic membrane exocytosis protein 1	Rims1	0.013166844
Q9WV18	Gamma-aminobutyric acid type B receptor subunit 1	Gabbr1	0.016828527
Q9DBS2	Tumor protein p63-regulated gene 1-like protein	Tprg1l	0.020684394
Q80TJ1	Calcium-dependent secretion activator 1	Cadps	0.023937239
Q61016	Guanine nucleotide-binding protein subunit gamma-7	Gng7	0.031149121
Q62443	Neuronal pentraxin-1	Nptx1	0.049087128
	Mitochondrial function		
P97807	Fumarate hydratase, mitochondrial	Fh	1.89049E-05
Q8BKZ9	Pyruvate dehydrogenase protein X component	Pdhx	0.000182343
Q8BFR5	Elongation factor Tu, mitochondrial	Tufm	0.000219998
Q8BH59	Calcium-binding mitochondrial carrier protein Aralar1	Slc25a12	0.000343059
O08749	Dihydrolipoyl dehydrogenase, mitochondrial	Dld	0.001059691
Q99KB8	Hydroxyacylglutathione hydrolase, mitochondrial	Hagh	0.001154019
Q60930	Voltage-dependent anion-selective channel protein 2	Vdac2	0.003519833
Q9JHI5	Isovaleryl-CoA dehydrogenase, mitochondrial	Ivd	0.003828896
Q61941	NAD(P) transhydrogenase, mitochondrial	Nnt	0.004299233
P70404	Isocitrate dehydrogenase [NAD] subunit gamma 1	Idh3g	0.005805916
O35143	ATPase inhibitor, mitochondrial	Atp5if1	0.006163506
Q5NCE8	Magnesium transporter MRS2 homolog, mitochondrial	Mrs2	0.009684623
Q9D051	Pyruvate dehydrogenase E1 component subunit beta	Pdhb	0.011119372
Q9JLZ3	Methylglutaconyl-CoA hydratase, mitochondrial	Auh	0.011503073
Q9CPZ8	COX assembly mitochondrial protein homolog	Cmc1	0.011903721
Q9DCC8	Mitochondrial import receptor subunit TOM20 homolog	Tomm20	0.013691041
P51174	Long-chain specific acyl-CoA dehydrogenase	Acadl	0.014069291
Q07417	Short-chain specific acyl-CoA dehydrogenase	Acads	0.014588163
Q9JIY5	Serine protease HTRA2, mitochondrial	Htra2	0.01537337
Q8BGX2	Mitochondrial import membrane translocase (Tim29)	Timm29	0.017629493
Q9WVA2	Mitochondrial import membrane translocase (Tim8A)	Timm8a1	0.020053563
Q9D7B6	Isobutyryl-CoA dehydrogenase, mitochondrial	Acad8	0.022488468
O08600	Endonuclease G, mitochondrial	Endog	0.02435898
P47738		Aldh2	0.025395545

(*continued on next page*)

Table 1 (*continued*)

Accession	Protein Name	Gene Name	P value
	Aldehyde dehydrogenase, mitochondrial		
O35857	Mitochondrial import membrane translocase (Tim44)	Timm44	0.025846245
Q6PE15	Mycophenolic acid acyl-glucuronide esterase	Abhd10	0.028842325
Q3UMR5	Calcium uniporter protein, mitochondrial	Mcu	0.033233774
Q9Z2I9	Succinate–CoA ligase [ADP-forming] subunit beta	Sucla2	0.040013037
P30275	Creatine kinase U-type, mitochondrial	Ckmt1	0.041798187
Q8CGK3	Lon protease homolog, mitochondrial	Lonp1	0.047715831
	Protein synthesis and degradation		
Q8BP47	Asparagine–tRNA ligase, cytoplasmic	NARS1	0.000134471
Q9DD18	D-aminoacyl-tRNA deacylase 1	Dtd1	0.002840307
Q9Z127	Large neutral amino acids transporter small subunit 1	Slc7a5	0.003859166
Q922B2	Aspartate–tRNA ligase, cytoplasmic	Dars1	0.004177611
Q64213	Splicing factor 1	Sf1	0.0071075
P61202	COP9 signalosome complex subunit 2	Cops2	0.013009051
Q9ER72	Cysteine–tRNA ligase, cytoplasmic	Cars1	0.015261375
Q9Z1X4	Interleukin enhancer-binding factor 3	Ilf3	0.02768796
O70194	Eukaryotic translation initiation factor 3 subunit D	Eif3d	0.029492568
Q3U0V1	Far upstream element-binding protein 2	Khsrp	0.037898617
Q06890	Clusterin	Clu	0.037847887
Q99PL6	UBX domain-containing protein 6	Ubxn6	0.036924509
Q8K0B2	Lysosomal cobalamin transport escort protein LMBD1	Lmbrd1	0.038995409
Q9R0P9	Ubiquitin carboxyl-terminal hydrolase isozyme L1	Uchl1	0.044148581
Q80X50	Ubiquitin-associated protein 2-like	Ubap2l	0.044849063
	Cytoskeleton and transport		
O35098	Dihydropyrimidinase-related protein 4	Dpysl4	9.41366E-05
Q3UVL4	Vacuolar protein sorting-associated protein 51 homolog	Vps51	0.000644658
Q9D898	Actin-related protein 2/3 complex subunit 5-like protein	Arpc5l	0.00114265
P70206	Plexin-A1	Plxna1	0.001259489
Q3UHB8	Coiled-coil domain-containing protein 177	Ccdc177	0.002273706
Q60598	Src substrate cortactin	Cttn	0.002443861
Q9QXT0	Protein canopy homolog 2	Cnpy2	0.00260753
P61027	Ras-related protein Rab-10	Rab10	0.003205837
Q9D1D4	Transmembrane emp24 domain-containing protein 10	Tmed10	0.003931995
Q7TQD2	Tubulin polymerization-promoting protein	Tppp	0.003942978
O35382	Exocyst complex component 4	Exoc4	0.004170172
Q8K4G5	Actin-binding LIM protein 1	Ablim1	0.004307204
A2A5R2	Brefeldin A-inhibited guanine exchange protein 2	Arfgef2	0.005885931
Q80U49	Centrosomal protein of 170 kDa protein B	Cep170b	0.007734822
Q8CHU3	Epsin-2	Epn2	0.009808381
Q9QYX7	Protein piccolo	Pclo	0.008826
Q5SSM3	Rho GTPase-activating protein 44	Arhgap44	0.012362
Q62417	Sorbin and SH3 domain-containing protein 1	Sorbs1	0.012625649
P45591	Cofilin-2	Cfl2	0.012924261
P68373	Tubulin alpha-1C chain	Tuba1c	0.013120303
D3YZU1	SH3 and multiple ankyrin repeat domains protein 1	Shank1	0.017417306
Q61301	Catenin alpha-2	Ctnna2	0.019164554
Q8VHE6	Dynein heavy chain 5, axonemal	Dnah5	0.019527187
Q9Z0R6	Intersectin-2	Itsn2	0.0231552
Q9ET54	Palladin	Palld	0.02616493
Q8CHC4	Synaptojanin-1	Synj1	0.027750155
O08638	Myosin-11	Myh11	0.02778766
Q9JIG8	PRA1 family protein 2	Praf2	0.030217925
P47757	F-actin-capping protein subunit beta	Capzb	0.030845069
P61022	Calcineurin B homologous protein 1	Chp1	0.034691636
Q61548	Clathrin coat assembly protein AP180	Snap91	0.034725117
Q9JM76	Actin-related protein 2/3 complex subunit 3	Arpc3	0.03908293

Table 1 (*continued*)

Accession	Protein Name	Gene Name	P value
Q9JM96	Cdc42 effector protein 4	Cdc42ep4	0.041125024
Q8C754	Vacuolar protein sorting-associated protein 52 homolog	Vps52	0.041757532
P63044	Vesicle-associated membrane protein 2	Vamp2	0.044359734
Q91W86	Vacuolar protein sorting-associated protein 11 homolog	Vps11	0.045630805
Q69Z23	Dynein heavy chain 17, axonemal	Dnah17	0.047492131
Q9EPJ9	ADP-ribosylation factor GTPase-activating protein 1	Arfgap1	0.049281009
	Signal transduction		
P47809	Dual specificity mitogen-activated kinase kinase 4	Map2k4	0.000582444
Q9JI46	Diphosphoinositol polyphosphate phosphohydrolase 1	Nudt3	0.002056375
Q60676	Serine/threonine-protein phosphatase 5	Ppp5c	0.002672554
Q8R071	Inositol-trisphosphate 3-kinase A	Itpka	0.003906467
Q61036	Serine/threonine-protein kinase PAK 3	Pak3	0.005076213
P97797	Tyrosine-phosphatase non-receptor type substrate 1	Sirpa	0.009320041
Q9D7X3	Dual specificity protein phosphatase 3	Dusp3	0.009359351
B9EKR1	Receptor-type tyrosine-protein phosphatase zeta	Ptprz1	0.00970121
Q5F2E8	Serine/threonine-protein kinase TAO1	Taok1	0.012456841
Q63739	Protein tyrosine phosphatase type IVA 1	Ptp4a1	0.012659917
O54833	Casein kinase II subunit alpha'	Csnk2a2	0.013136094
P08414	Calcium/calmodulin-dependent protein kinase type IV	Camk4	0.013190381
Q4JIM5	Tyrosine-protein kinase ABL2	Abl2	0.013218866
Q6P4S6	Serine/threonine-protein kinase SIK3	Sik3	0.015454386
P51830	Adenylate cyclase type 9	Adcy9	0.017368072
Q01065	Ca^{++}/calmodulin-dep.nucleotide phosphodiesterase 1B	Pde1b	0.019071468
Q58A65	C-Jun-amino-terminal kinase-interacting protein 4	Spag9	0.029496127
Q68FM6	Protein phosphatase 1 regulatory subunit 29	Elfn2	0.030278896
Q8CHP8	Glycerol-3-phosphate phosphatase	Pgp	0.036035811
Q61481	Ca^{++}/calmodulin-dep.nucleotide phosphodiesterase 1A	Pde1a	0.036920851
O08586	Phosphatidylinositol 3,4,5-trisphosphate 3-phosphatase and dual-specificity protein phosphatase	Pten	0.03799829
P84309	Adenylate cyclase type 5	Adcy5	0.040467549
Q04690	Neurofibromin	Nf1	0.046269791
Q9DCB4	cAMP-regulated phosphoprotein 21	Arpp21	0.048266949

Aβ1-42 (Fig. 4B). In order to assess whether the pro-inflammatory effect of Aβ1-42 is associated with increased cell death, apoptosis and necrosis were tested by Annexin V/propidium iodide (PI) staining. These experiments showed no significant changes in cell apoptosis and necrosis as a consequence of Aβ1-42 treatment (Fig. 4C).

3.3. *Amyloid peptide beta causes NOX1-dependent oxidative stress in endothelial cells*

In order to understand the molecular nature of the inflammatory injury of endothelial cells by Aβ1-42, we used electron paramagnetic resonance spectroscopy. CMH was used as superoxide anion-specific spin probe (Supplementary Fig. 1) [33]. Using this technique, we were able to show that Aβ1-42 results in a dose-dependent increase in superoxide anion generation in HUVECs, reaching a significant increase at both 10 and 25 μM when compared to the scrambled peptide (Fig. 5A). Next, we used the NOX-specific inhibitor VAS2870 [36] to identify NOXs as the source of the oxidative burst induced by in HUVECs (Fig. 5B). The use of a highly selective NOX1 inhibitory peptide [37] allowed us to pinpoint NOX1 as the most relevant source of superoxide anion in response to Aβ1-42 (Fig. 5B). In order to confirm this finding, we used siRNA transfection to silence the genes of the four NOX enzymes

Table 2
Selected differentially expressed proteins in the hippocampus of 3xTG-AD mice at 12 months of age divided by cellular function. The statistical significance of the difference was tested by Student T-test (n = 6).

Accession	Protein Name	Gene Name	P value
	Redox Homeostasis		
Q9D1X0	Nucleolar protein 3	Nol3	0.0004100
Q9JJK2	LanC-like protein 2	Lancl2	0.0025878
Q8BMF3	NADP-dependent malic enzyme, mitochondrial	Me3	0.0037963
Q61578	NADPH:adrenodoxin oxidoreductase, mitochondrial	Fdxr	0.0102717
P51855	Glutathione synthetase	Gss	0.0145300
Q4KMM3	Oxidation resistance protein 1	Oxr1	0.0204491
Q64133	Amine oxidase [flavin-containing] A	Maoa	0.0224494
Q8K097	Protein lifeguard 2	Faim2	0.0270026
Q8BR63	Protein FAM177A1	Fam177a1	0.0326738
Q9R257	Heme-binding protein 1	Hebp1	0.0358492
Q9DB73	NADH-cytochrome b5 reductase 1	Cyb5r1	0.0493211
	Neurotransmission		
Q9CXP8	Guanine nucleotide-binding protein subunit gamma-10	Gng10	1.8577E-06
Q61016	Guanine nucleotide-binding protein subunit gamma-7	Gng7	0.0003138
O08599	Syntaxin-binding protein 1	Stxbp1	0.0008032
P61264	Syntaxin-1B	Stx1b	0.0035973
Q62442	Vesicle-associated membrane protein 1	Vamp1	0.0043429
Q8BLE7	Vesicular glutamate transporter 2	Slc17a6	0.0049574
Q63959	Potassium voltage-gated channel subfamily C member 3	Kcnc3	0.0168435
P12961	Neuroendocrine protein 7B2	Scg5	0.0087150
Q9JIS5	Synaptic vesicle glycoprotein 2A	Sv2a	0.0192159
O35633	Vesicular inhibitory amino acid transporter	Slc32a1	0.0365301
P46097	Synaptotagmin-2	Syt2	0.0458441
P60761	Neurogranin	Nrgn	0.0463479
Q80U57	Regulating synaptic membrane exocytosis protein 3	Rims3	0.0492523
	Mitochondrial function		
P26443	Glutamate dehydrogenase 1, mitochondrial	Glud1	0.0011715
Q8BWT1	3-ketoacyl-CoA thiolase, mitochondrial	Acaa2	0.0012530
Q9JHI5	Isovaleryl-CoA dehydrogenase, mitochondrial	Ivd	0.0013191
Q9Z2I9	Succinate–CoA ligase [ADP-forming] subunit beta	Sucla2	0.0016019
Q9D0K2	Succinyl-CoA:3-ketoacid coenzyme A transferase 1	Oxct1	0.0056800
Q9CQJ8	NADH dehydrogenase [ubiquinone] 1 beta subunit 9	Ndufb9	0.0062625
Q64521	Glycerol-3-phosphate dehydrogenase, mitochondrial	Gpd2	0.0068882
Q9D2G2	Dihydrolipoyllysine-residue succinyltransferase, mit.	Dlst	0.0071909
P99028	Cytochrome *b*-*c*1 complex subunit 6, mitochondrial	Uqcrh	0.0086600
Q9QYA2	Mitochondrial import receptor subunit TOM40 homolog	Tomm40	0.0089307
P51174	Long-chain specific acyl-CoA dehydrogenase, mit.	Acadl	0.0098817
Q80U63	Mitofusin-2	Mfn2	0.0110611
Q9DC61	Mitochondrial-processing peptidase subunit alpha	Pmpca	0.0151678
Q99JR1	Sideroflexin-1	Sfxn1	0.0170387
Q9CPW3	39S ribosomal protein L54, mitochondrial	Mrpl54	0.0192249
Q5NCE8	Magnesium transporter MRS2 homolog, mitochondrial	Mrs2	0.0196724
P58281	Dynamin-like 120 kDa protein, mitochondrial	Opa1	0.0198544
Q9CQ92	Mitochondrial fission 1 protein	Fis1	0.0235869
Q99JB2	Stomatin-like protein 2, mitochondrial	Stoml2	0.0245708
Q9CXT8	Mitochondrial-processing peptidase subunit beta	Pmpcb	0.0250706
Q8BGX2	Mitochondrial import membrane translocase (Tim29)	Timm29	0.0259164
Q9CPU2	NADH dehydrogenase 1 beta subcomplex subunit 2	Ndufb2	0.0286871
Q8BFR5	Elongation factor Tu, mitochondrial	Tufm	0.0309189
Q8BVU5	ADP-ribose pyrophosphatase, mitochondrial	Nudt9	0.0339598
Q9CR21	Acyl carrier protein, mitochondrial	Ndufab1	0.0343109
Q9CZ13	Cytochrome *b*-*c*1 complex subunit 1, mitochondrial	Uqcrc1	0.0346424
Q9CTY5	Calcium uptake protein 3, mitochondrial	Micu3	0.0350402
P97807	Fumarate hydratase, mitochondrial	Fh	0.0374148
Q9WVA2	Mitochondrial import membrane translocase (Tim8A)	Timm8a1	0.0378318
Q8C163	Nuclease EXOG, mitochondrial	Exog	0.0395071
Q61941	NAD(P) transhydrogenase, mitochondrial	Nnt	0.0412028
	Protein synthesis and degradation		
Q9Z127	Large neutral amino acids transporter small subunit 1	Slc7a5	0.0000471
O35286	Pre-mRNA-splicing factor ATP-dependent RNA helicase DHX15	Dhx15	0.0001885
Q9R0P9	Ubiquitin carboxyl-terminal hydrolase isozyme L1	Uchl1	0.0005190
Q8CHW4	Translation initiation factor eIF-2B subunit epsilon	Eif2b5	0.0009779
O89086	RNA-binding protein 3	Rbm3	0.0009883
Q06890	Clusterin	Clu	0.0013534
Q61035	Histidine–tRNA ligase, cytoplasmic	Hars1	0.0015495
Q9CZR8	Elongation factor Ts, mitochondrial	Tsfm	0.0019621
Q9CX86	Heterogeneous nuclear ribonucleoprotein A0	Hnrnpa0	0.0024443
P14206	40S ribosomal protein SA	Rpsa	0.0045845
Q99MN1	Lysine–tRNA ligase	Kars1	0.0081983
Q8BP47	Asparagine–tRNA ligase, cytoplasmic	NARS1	0.0091134
Q8K0B2	Lysosomal cobalamin transport escort protein LMBD1	Lmbrd1	0.0095729
Q8BGQ7	Alanine–tRNA ligase, cytoplasmic	Aars1	0.0102687
Q80X50	Ubiquitin-associated protein 2-like	Ubap2l	0.0116174
Q8BJW6	Eukaryotic translation initiation factor 2A	Eif2a	0.0116343
Q69ZR2	E3 ubiquitin-protein ligase HECTD1	Hectd1	0.0119589
Q9JK81	MYG1 exonuclease	Myg1	0.0143308
Q9CQJ6	Density-regulated protein	Denr	0.0216944
Q9DBR3	Armadillo repeat-containing protein 8	Armc8	0.0220314
Q91YR5	eEF1A lysine and N-terminal methyltransferase	EEF1A	0.0232695
Q8K2H2	Deubiquitinase OTUD6B	Otud6b	0.0249278
Q8CFI0	E3 ubiquitin-protein ligase NEDD4-like	Nedd4l	0.0294142
Q6I6G8	E3 ubiquitin-protein ligase HECW2	Hecw2	0.0298136
Q3THG9	Alanyl-tRNA editing protein Aarsd1	Aarsd1	0.0370224
O35226	26S proteasome non-ATPase regulatory subunit 4	Psmd4	0.0413585
P70398	Probable ubiquitin carboxyl-terminal hydrolase FAF-X	Usp9x	0.0413649
Q99NB8	Ubiquilin-4	Ubqln4	0.0455887
Q9CZD3	Glycine–tRNA ligase	Gars1	0.0460988
Q8R1B4	Eukaryotic translation initiation factor 3 subunit C	Eif3c	0.0463175
Q9D0L8	mRNA cap guanine-N7 methyltransferase	Rnmt	0.0494536
	Cytoskeleton and transport		
Q6ZWY8	Thymosin beta-10	Tmsb10	0.0000772
Q8BMK4	Cytoskeleton-associated protein 4	Ckap4	0.0001625
Q8CJ19	[F-actin]-monooxygenase MICAL3	Mical3	0.0154730
P08553	Neurofilament medium polypeptide	Nefm	0.0159967
Q7TSJ2	Microtubule-associated protein 6	Map6	0.0160480
Q80VC9	Calmodulin-regulated spectrin-associated protein 3	Camsap3	0.0166943
Q9JMH9	Unconventional myosin-XVIIIa	Myo18a	0.0167323
Q9Z0Y1	Dynactin subunit 3	Dctn3	0.0170890
O35098	Dihydropyrimidinase-related protein 4	Dpysl4	0.0180992
P33173	Kinesin-like protein KIF1A	Kif1a	0.0248401
Q8VHI6	Wiskott-Aldrich syndrome protein family member 3	Wasf3	0.0290168
Q9JI91	Alpha-actinin-2	Actn2	0.0304053
P61294	Ras-related protein Rab-6B	Rab6b	0.0378387
Q91VR7		Map1lc3a	0.0384922

(*continued on next page*)

Table 2 (*continued*)

Accession	Protein Name	Gene Name	P value
	Microtubule-associated proteins 1A/1B light chain 3A		
Q9D1D4	Transmembrane emp24 domain-containing protein 10	Tmed10	0.0459261
	Signal transduction		
Q69Z98	Serine/threonine-protein kinase BRSK2	Brsk2	0.0047860
Q01065	Ca^{++}/calmodulin-dependent phosphodiesterase 1B	Pde1b	0.0057916
Q61481	Ca^{++}/calmodulin-dependent phosphodiesterase 1A	Pde1a	0.0092916
Q6Q477	Plasma membrane calcium-transporting ATPase 4	Atp2b4	0.0094767
Q9JI46	Diphosphoinositol polyphosphate phosphohydrolase 1	Nudt3	0.0095734
Q5EG47	5′AMP-activated protein kinase subunit alpha-1	Prkaa1	0.0102116
P63328	Serine/threonine-protein phosphatase 2B catalytic subunit alpha isoform	Ppp3ca	0.0141343
P84309	Adenylate cyclase type 5	Adcy5	0.0196851
O89084	cAMP-specific 3′,5′-cyclic phosphodiesterase 4A	Pde4a	0.0231420
Q61074	Protein phosphatase 1G	Ppm1g	0.0237536
Q8BW96	Calcium/calmodulin-dependent protein kinase type 1D	Camk1d	0.0257440
Q8R2U6	Diphosphoinositol polyphosphate phosphohydrolase 2	Nudt4	0.0268370
P58389	Serine/threonine-protein phosphatase 2A activator	Ptpa	0.0274647
Q9Z2H2	Regulator of G-protein signaling 6	Rgs6	0.0297922
Q5SSL4	Active breakpoint cluster region-related protein	Abr	0.0301602
Q9CQV8	14-3-3 protein beta/alpha	Ywhab	0.0306698
Q9DBC7	cAMP-dep. protein kinase type I-alpha reg. subunit	Prkar1a	0.0316314
Q60829	Protein phosphatase 1 regulatory subunit 1B	Ppp1r1b	0.0336775
Q58A65	C-Jun-amino-terminal kinase-interacting protein 4	Spag9	0.0331436
Q80TS3	Adhesion G protein-coupled receptor L3	Adgrl3	0.0343670
Q9D967	Magnesium-dependent phosphatase 1	Mdp1	0.0364410
P84075	Neuron-specific calcium-binding protein hippocalcin	Hpca	0.0425279
P05480	Neuronal proto-oncogene tyrosine-protein kinase Src	Src	0.0425946
Q6NS52	Diacylglycerol kinase beta	Dgkb	0.0429672
Q8CGK7	Guanine nucleotide-binding protein G (olf) subunit alpha	Gnal	0.0431162
Q8CGA0	Protein phosphatase 1F	Ppm1f	0.0432068
Q3UMT1	Protein phosphatase 1 regulatory subunit 12C	Ppp1r12c	0.0456373
P41242	Megakaryocyte-associated tyrosine-protein kinase	Matk	0.0495276

expressed in endothelial cells (NOX1, NOX2, NOX4 or NOX5) [38]. The silencing of NOX1 almost completely abolished the Aβ1-42-dependent increase in superoxide anion generation (Fig. 5C), while the silencing of other NOXs had no significant effect. The efficiency of siRNA silencing was assessed by RT-qPCR, which showed all 4 siRNA treatment significantly reducing the expression of the targeted NOX enzymes by at least 70% (Supplementary Fig. 2). In order to test whether the Aβ1-42 treatment upregulates the expression of NOX enzymes (which could explain the increase in superoxide anion generation), NOX1, NOX2, NOX4 and NOX5 were quantified by RT-qPCR following the treatment with Aβ1-42. None of the above enzyme was significantly upregulated by Aβ1-42 (Fig. 5D). The importance of NOX1 in the oxidative stress induced by Aβ1-42 in HUVECs was also confirmed by experiments where the expression of the oxidative stress marker HO-1 was tested by RT-qPCR (Supplementary Fig. 3). In these experiments, the silencing of NOX1 abolished the HO-1 upregulation caused by Aβ1-42.

3.4. Amyloid peptide beta impairs the barrier function of endothelial cells in endothelial cells

Using electric cell-substrate impedance sensing (ECIS) we tested the barrier functions of HUVECs treated with Aβ peptide, which is proportional to the electric impedance of cell monolayers measured at frequency 4000 Hz. After the initial 24 h to allow the formation of a complete monolayer, treatment with the Aβ1-42 peptide for further 24 h (up to t = 48 h) reduced electrical impedance as a consequence of intercellular junction loosening and loss barrier function (Fig. 6A). We then induced electrical damage of the monolayer by electrical wounding and assessed monolayer electrical impedance for further 24 h (up to t = 72 h), which measures the ability of cells to migrate and reform a complete monolayer. The cells treated with Aβ1-42 peptide were unable to heal after wounding, leading to persistent low impedance 24 h after wounding compared to cells treated with the scrambled control peptide. Using immunocytochemistry experiments, we showed that the impaired barrier function is associated with a reduction in the localisation of the intercellular junction protein VE-cadherin at the cellular edge (Fig. 6B). The assessment of the phosphorylation state of VE-cadherin by immunoblotting allowed us to detect a significantly increased level of VE-cadherin phosphorylation at tyrosine 658 (Y658) in response to Aβ1-42 peptide compared to scrambled control peptide (Fig. 6C). Next, we investigated the molecular mechanisms underlying the loss of endothelial barrier function induced by the Aβ1-42 peptide. The NOX inhibition with the pan inhibitor VAS2870 (Fig. 7A) and the NOX1-selective abolishment of oxidative stress with the selective inhibitory peptide NoxA1ds (Fig. 7B) protected HUVECs from the injury caused by Aβ1-42 peptide. Both pre-wounding barrier function and post-wounding barrier repair were preserved when NOX1 was inhibited, while the scrambled control peptide for NoxA1ds had no effect compared to untreated cells (shown in Fig. 7A). In order to confirm that the effect on endothelial monolayer impedance corresponded to a change in permeability, we performed experiments with FITC-albumin as a tracer. As shown in Fig. 7C, HUVEC treatment with Aβ1-42 led to an increase in monolayer permeability (which was statistically significant at 24 h and 48 h after treatment). The selective inhibitory peptide NoxA1ds abolished the increase in HUVEC permeability caused by Aβ1-42.

3.5. Aβ peptide causes barrier function damage in hBMECs in a NOX1-dependent manner

In order to confirm the physiopathological relevance of our findings obtained with HUVECs, we repeated key experiments with the primary human cerebrovascular endothelial cells hBMECs. As for HUVEC experiments, also in primary human brain endothelial cells, we used NoxA1ds peptide to selectively inhibit NOX1. In Fig. 8A, similarly to what we observed in HUVECs, we present data showing that Aβ1-42 induces VE-cadherin phosphorylation (Y658) in hBMECs. Moreover, Aβ1-42 stimulates a significant increase in superoxide generation (compared to scrambled peptide) (Fig. 8B). The pre-treatment of hBMECs with the NoxA1ds peptide inhibited in a comprehensive and statistically significant manner this superoxide anion burst, suggesting that the Aβ1-42 peptide treatment induces the activation of NOX1 also is this endothelial cell type. We were then able to confirm the loss in hBMEC barrier function following Aβ1-42 treatment and its NOX1-dependence. In Fig. 8C, we show that Aβ1-42 treatment causes a significant loss in impedance in ECIS experiments compared to scrambled control peptide both before and after wounding. When we inhibited NOX1 using the NoxA1ds, the Aβ1-42-dependent loss in barrier function was abolished. The protective effect of NoxA1ds was more evident before monolayer wounding, but statistically significant after wounding as well. In order to confirm that the effect on hBMEC monolayer impedance corresponded to a change in permeability, we performed experiments with FITC-albumin as a tracer. As shown in Fig. 8D, hBMEC treatment with Aβ1-42 led to an increase in monolayer permeability

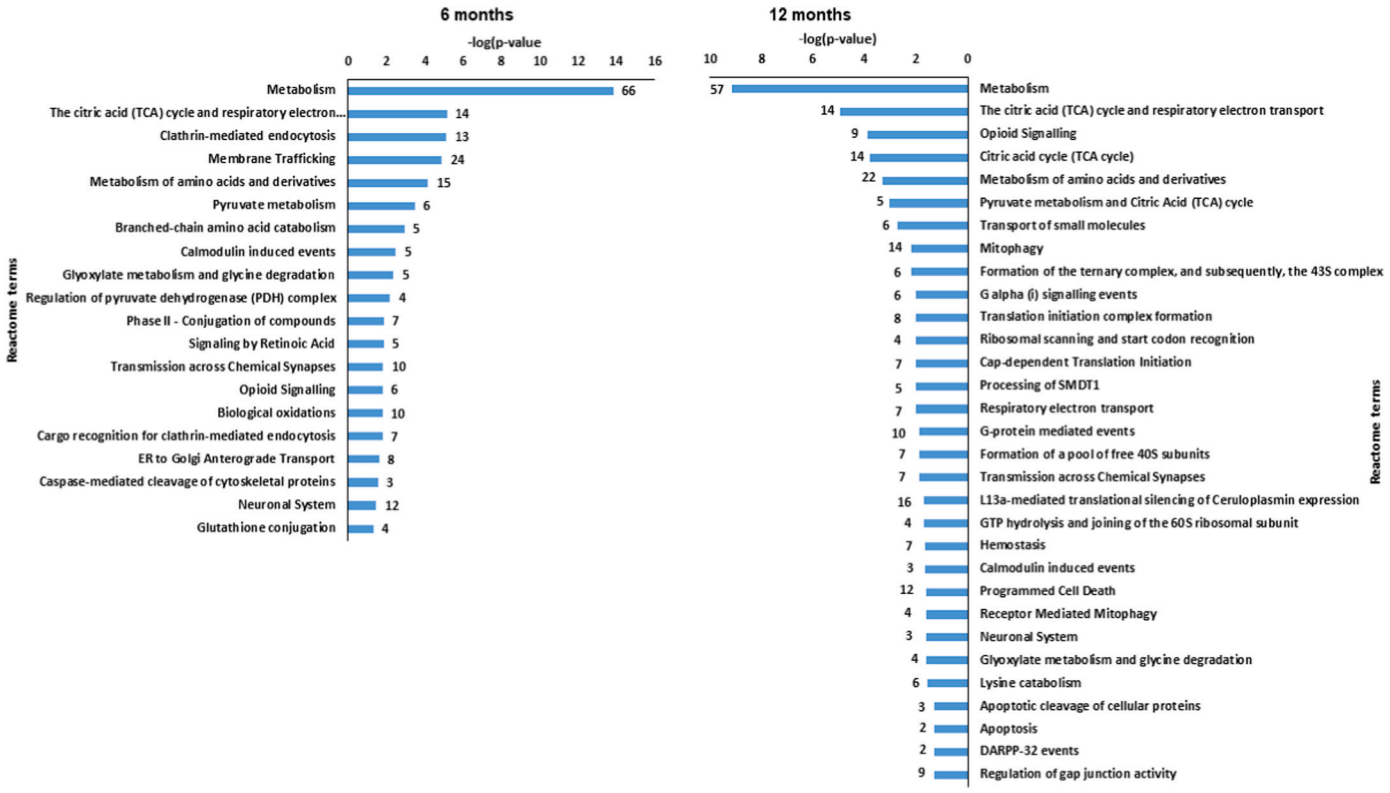

Fig. 2. Pathway analysis of proteomics results. STRING DB-based enrichment analysis of the Reactome database displaying cellular pathways with an enrichment p-value < 0.05. Proteins significantly different in 3xTG-AD mice at 6 months and 12 months of age compared to age matched controls (single protein p value < 0.05) were utilised for this analysis. Column label indicates number of proteins associated to the respective term or pathway.

(which was statistically significant at 24 h and 48 h after treatment). The selective inhibitory peptide NoxA1ds abolished the increase in hBMEC permeability caused by Aβ1-42.

4. Discussion

Despite some contrasting evidence [39], the impairment of the neurovasculature is suggested to contribute to the progression of neurodegeneration and dementia associated with AD [40,41]. Autopsy studies have shown that vascular alterations are present in the majority of clinically diagnosed AD cases [42]. The perivascular accumulation of amyloid peptide β in the brain is referred to as cerebral amyloid angiopathy (or CAA) [43,44]. CAA occurs in 85%–95% of AD patients, has a significant impact on neurovasculature function, and is considered an important contributor to AD [45]. Although some authors suggest that CAA only occurs at the later stages of the disease and leads to brain capillary rarefaction [46], the impairment of the neurovasculature is suggested to reduce clearance of amyloid peptide β and other toxic metabolites, and to limit oxygen and nutrient supply to the brain, which ultimately exacerbate neurodegeneration in AD [47]. Whether neurovascular degeneration plays a role in the early development of AD or its later stages of brain degeneration, its contribution to the disease is no longer disputed. It is therefore important to understand the effect of amyloid peptide β on vascular cells. In this study, following detection of markers of hippocampal oxidative stress by proteomics and the phosphorylation of the endothelial junctional protein VE-cadherin in a murine model of AD, we have focused on the oxidative damage of endothelial cell function caused by amyloid peptide β.

The 3xTG-AD mice used as a model of AD in this study were previously described for the intracerebral accumulation of amyloid peptide plaques from 6 months of age and cognitive decline starting at 9 months of age [28]. Here, we confirmed the formation of amyloid plaques from 6 months of age. Extensive changes in the brain proteome of murine AD models as a consequence of disease progression have been previously reported [48–50]. In this study, we focused on the proteomic changes in the hippocampus of these animals at 6 and 12 months of age compared to wild type controls. 224 and 228 proteins appeared differentially expressed, respectively. Based on the classification of the differentially-expressed proteins, mitochondrial function, protein synthesis/degradation and signal transduction appear as the most heavily affected cell functions at both 6 and 12 months of age, while cytoskeletal integrity seems more heavily affected at 6 months of age. Other cellular phenomena affected by the accumulation of amyloid peptide β in the hippocampus are neurotransmission, cell adhesion and redox homeostasis. Automated pathway analysis indicated metabolism (citric acid and amino acid pathways), membrane trafficking (including clathrin-mediated endocytosis), biological oxidations, and opioid signalling significantly affected in the hippocampus of 3xTG-AD mice. Cell degradative pathways such as apoptosis and mitophagy were significantly affected only at 12 months of age. A number of previous studies have utilised proteomics to identify pathological changes of the hippocampus in animal models of AD. A related mouse model characterised by two of the three mutations of 3xTG-AD mice (APP/PS1) displayed 231 protein changes compared to wild type controls of similar age (7 months) [51]. Similarly to our study, cytoskeletal integrity, mitochondrial function, protein turnover and cell signalling were the cellular functions more heavily affected. Other recent proteomics studies on the hippocampus of the APP/PS1 mouse model of AD show similarities with our results, with changes in proteins involved in protein turnover pathways (both synthesis and degradation) [52,53], neurotransmission [52], and, importantly, oxidative stress [53]. A key result of our proteomics study is in fact the identification of expression changes for proteins and enzymes associated with redox homeostasis, which suggests the possibility that the brain accumulation of amyloid peptide β leads to oxidative stress. This is in agreement with brain biochemistry studies suggesting that oxidative stress links amyloid peptide β accumulation

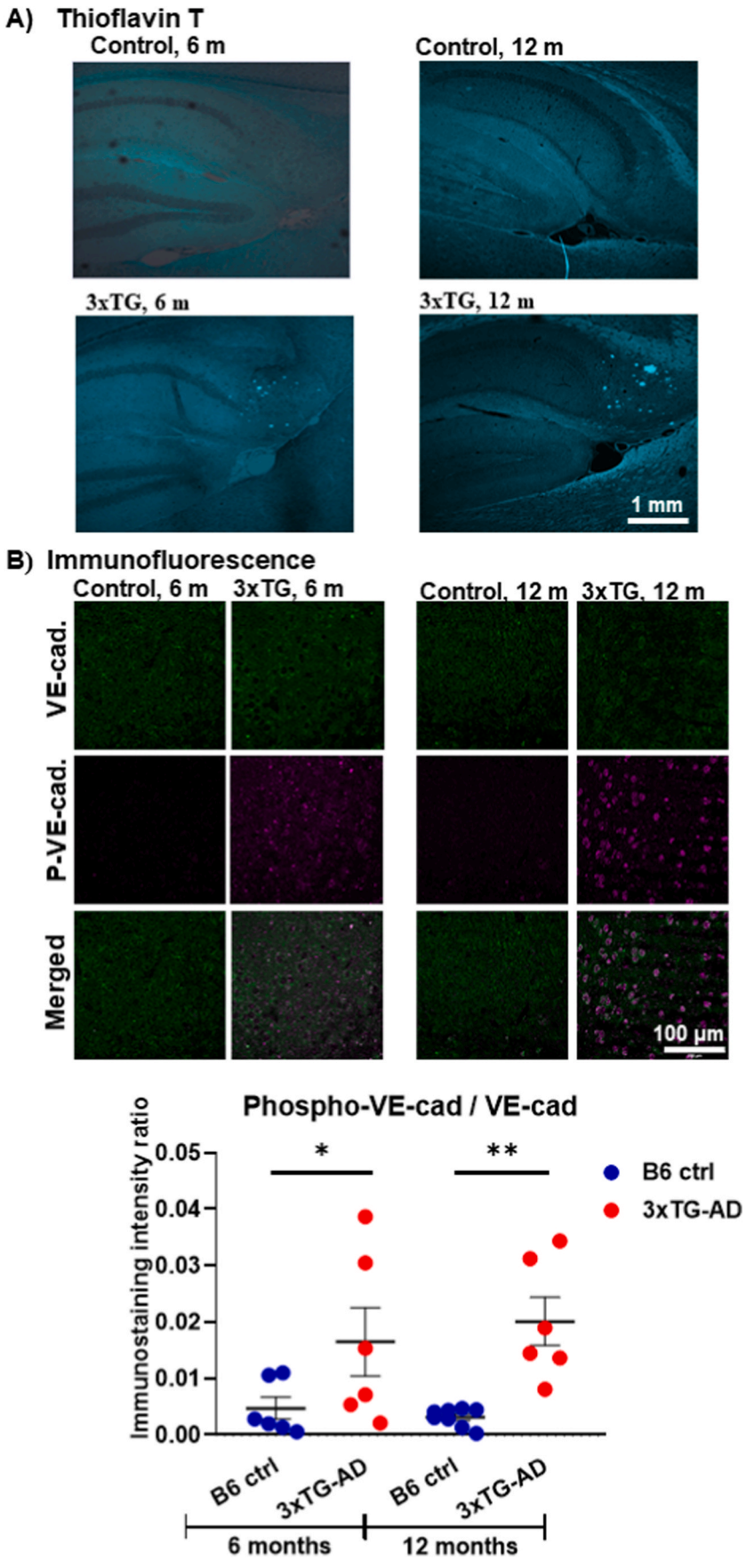

Fig. 3. Amyloid peptide β deposition and VE-cadherin hyperphosphorylation in the hippocampus of 3xTG-AD mice at 6 and 12 months of age. 3xTG-AD and B6129SF2 (wild type) mice were maintained for 6 or 12 months before fixation/perfusion, brain collection and tissue section. The amyloid peptide β deposition was visualised by Thioflavin T staining of the hippocampal region (A), while the immunostaining of the same region was performed with VE-cadherin and phospho-VE-cadherin antibodies (B). The images are representative of 6 mice per experimental group. The intensity of the phospho-VE-cadherin staining has been normalised to the intensity of the VE-cadherin staining. The statistical significance of the difference between 3xTG-AD and wild type mice at age 6 and 12 months was assessed by one-way ANOVA with Tukey post-test (*, $p < 0.05$; **, $p < 0.01$; ***, $p < 0.001$; $n = 6$).

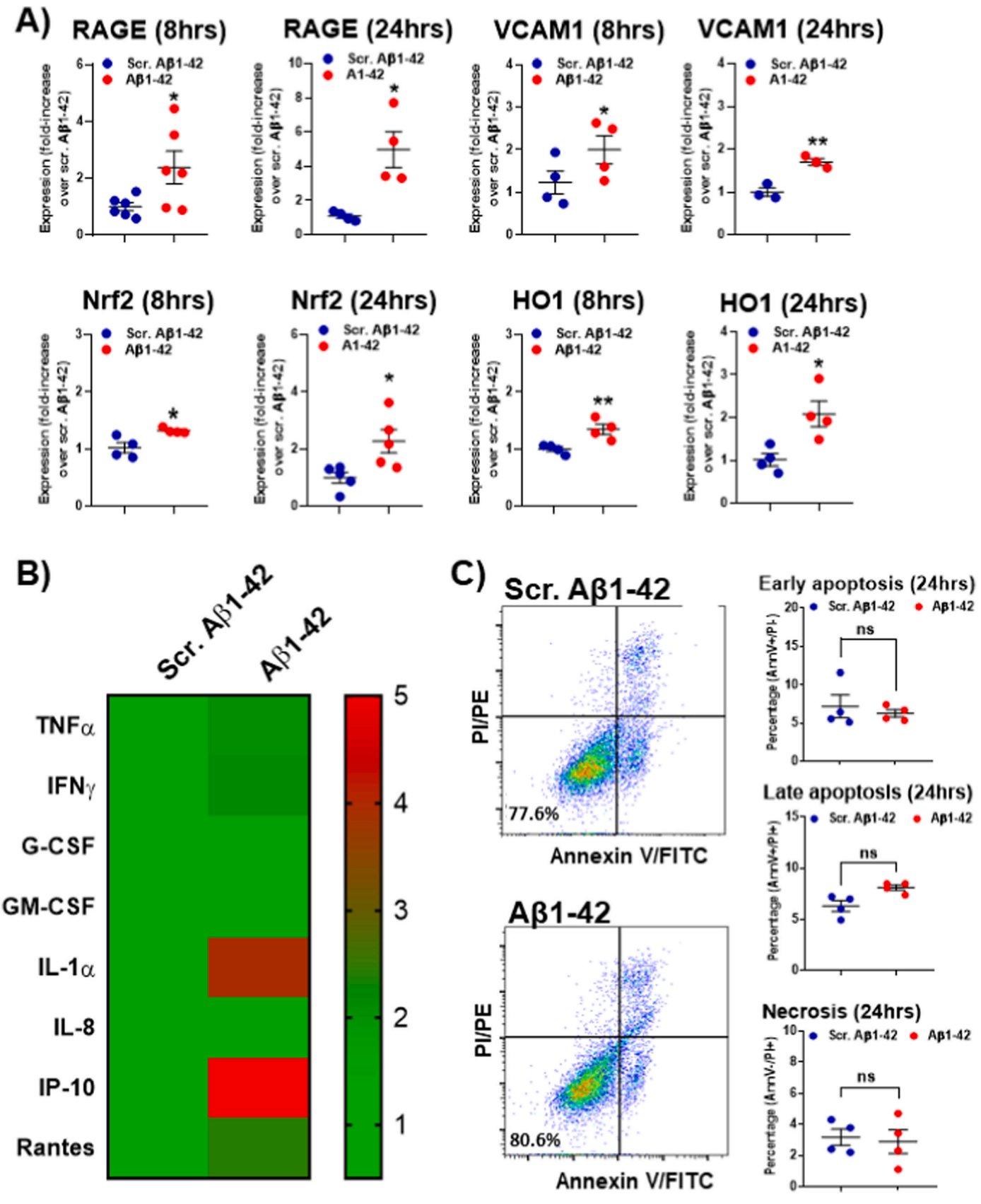

(caption on next page)

Fig. 4. Aβ1-42 causes pro-inflammatory changes in endothelial cells. HUVECs were treated with 25 μM Aβ1-42 or scrambled control peptide (scr. Aβ1-42) for 8 h or 24 h. RT-qPCR analysis shows that Aβ1-42 results in pro-inflammatory damage of endothelial cells as shown by significant upregulation of receptor for advanced glycation end products (RAGE), vascular cell adhesion protein 1 also known as vascular cell adhesion molecule 1 (VCAM-1), nuclear factor erythroid 2–related factor 2 (Nrf2) and Heme oxygenase-1 (HO-1) (Mann-Whitney non-parametric test: *, $p < 0.05$; **, $p < 0.01$; ***, $p < 0.001$; $n \geq 3$) (A). ELISA for pro-inflammatory cytokines shows > 2-fold increase for tumour necrosis factor α (TNF α), interferon γ (IFN-γ), interleukin-1α (IL-1α), IFN-γ-induced protein 10 (IP-10) and "regulated upon activation, normal T cell expressed and presumably secreted" (RANTES), as indicated by the heat map ($n = 3$) (B). Apoptosis assay for HUVECs treated with 25 μM Aβ1-42 or scrambled control peptide for 24 h was performed by flow cytometry (C). Annexin V/FITC + propidium iodide (PI) staining was utilised to assess early apoptotic (Annexin V^+/PI^-), late apoptotic (Annexin V^+/PI^+) and necrotic (Annexin V^-/PI^+) cells. Data are expressed as % of total events for the different quadrants. Statistical analysis was performed by Mann-Whitney non-parametric test (*, $p < 0.05$; **, $p < 0.01$; ***, $p < 0.001$; $n = 4$).

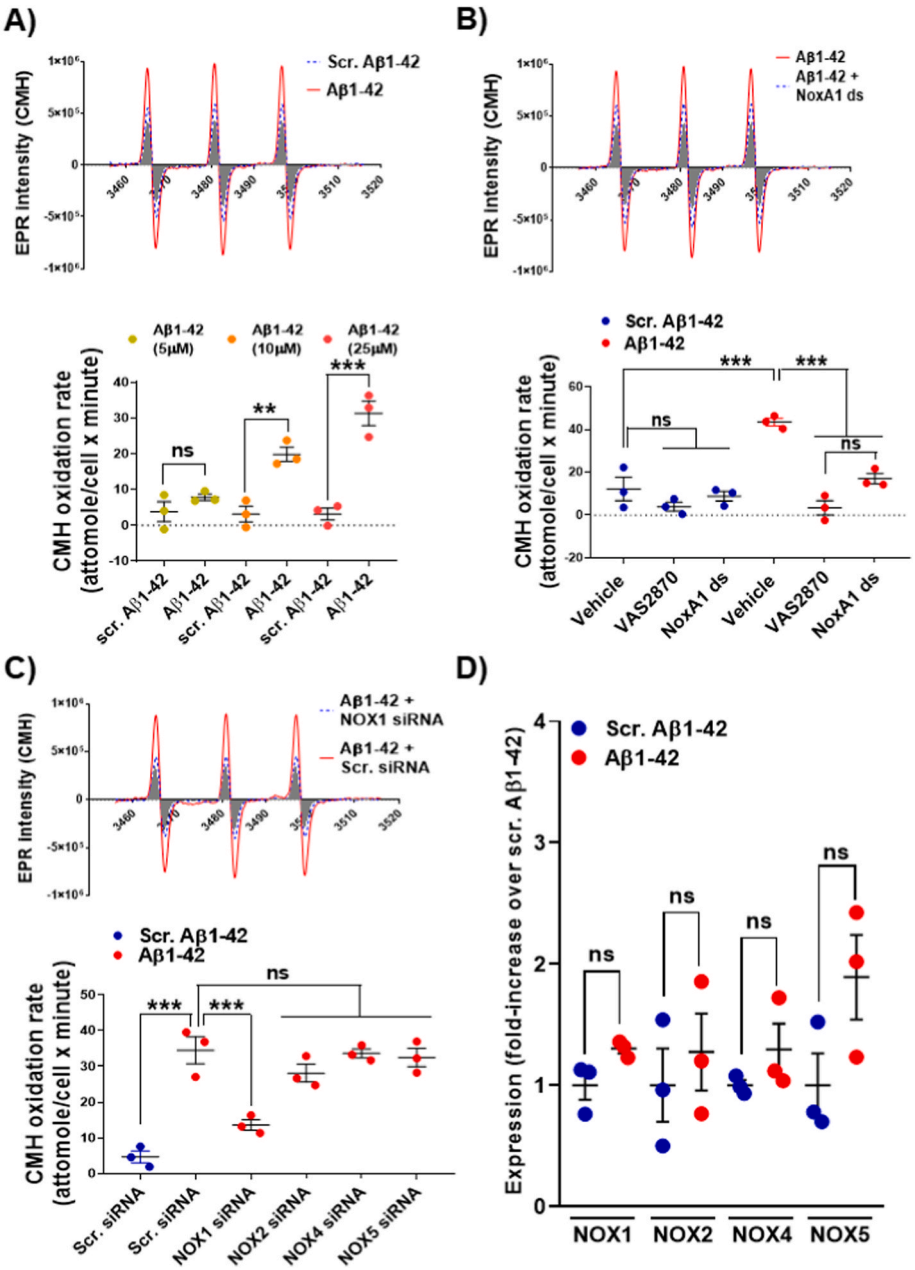

Fig. 5. Aβ1-42 stimulates the generation of superoxide anion in a NOX1-dependent manner. CMH was utilised for the detection of oxygen radicals generated by HUVECs following a 4 h treatment with 5, 10 or 25 μM Aβ1-42 or scrambled control peptide (scr. Aβ1-42) (A). The shaded area in the EPR trace represents untreated HUVEC cells. The NOX-specific inhibitor VAS2870 (10 μM) and the NOX1-selective peptide inhibitor NoxA1ds (10 μM) ablated the Aβ1-42-induced superoxide anion formation (B). The genetic silencing of NOX1, NOX2 NOX4 or NOX5 was achieved by siRNA transfection. The silencing of NOX1 significantly inhibited superoxide anion generation in response to the incubation with Aβ1-42 (C). Representative EPR traces are shown in the top panels of A-C (the shadowed traces represent the superoxide anion generation in the absence of peptide treatment). The effect of the treatment with 25 μM Aβ1-42 on NOX1, NOX2, NOX4, or NOX5 expression was tested by RT-qPCR as described in the methods (D). Throughout the figure, the statistical analysis was performed by one-way ANOVA with Tukey post-test and is shown in the bottom panels (*, $p < 0.05$; **, $p < 0.01$; ***, $p < 0.001$; $n = 3$).

and neurovascular damage [21,22]. The use of an alternative mouse model (i.e. 5XFAD) [54], also led to the discovery of the alteration of redox homeostasis pathways in the hippocampus in association with disease development (in particular, superoxide dismutases, which also appear amongst the changes on protein level associated to AD in our study) [55].

Because VE-cadherin is a protein expressed selectively by vascular endothelial cells [56], our data showing the phosphorylation of this protein in the brain of 3xTG-AD mice suggest an involvement of the vasculature in the changes associated with the onset or the progression of AD. It has previously been reported that tyrosine 658 phosphorylation of VE-cadherin controls vascular permeability and endothelial cell migration [57]. Our *in vitro* data confirm that amyloid peptide β impairs the barrier function of the endothelial monolayer and its repair after

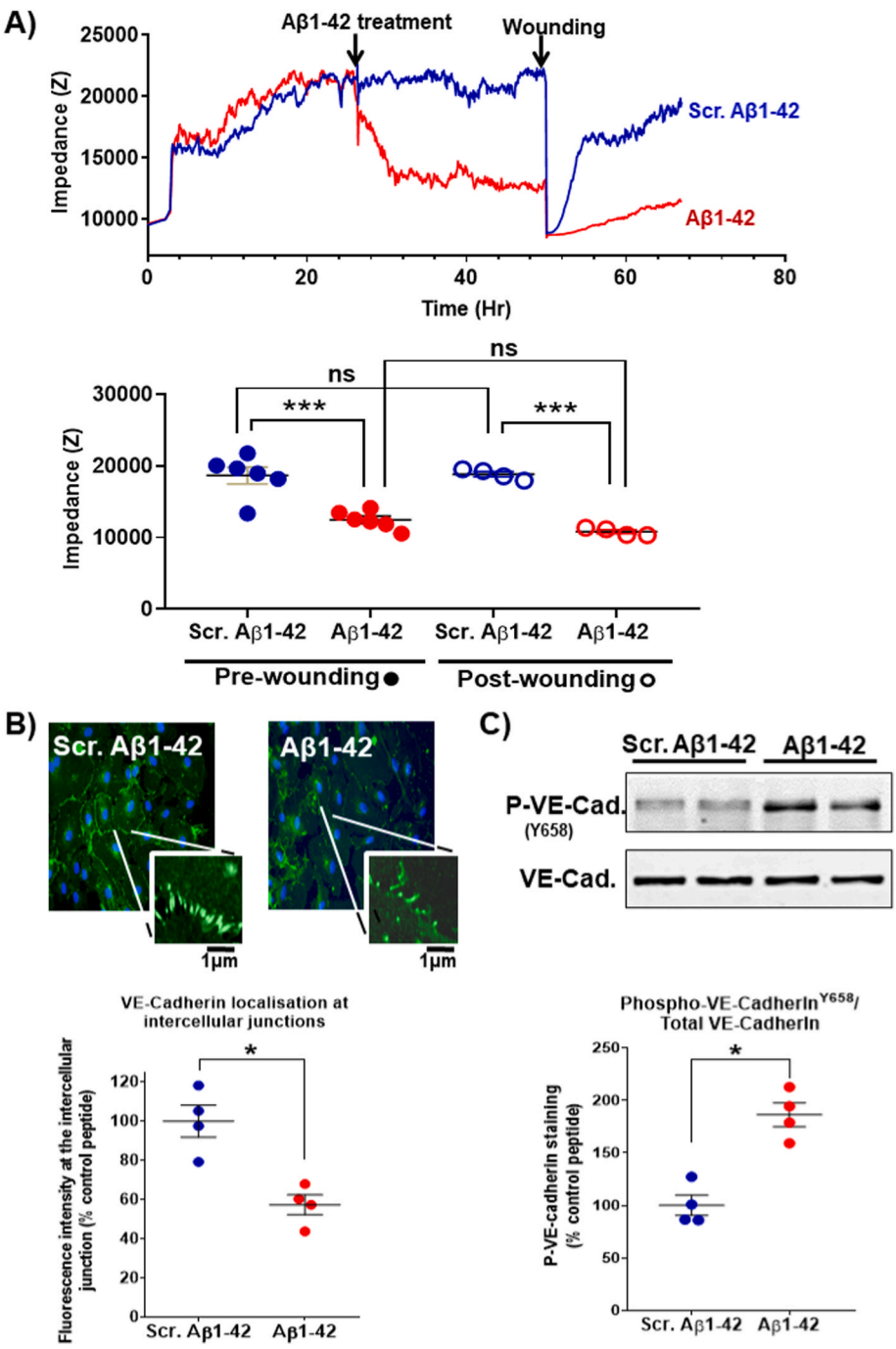

Fig. 6. Aβ1-42 causes barrier function impairment and VE-cadherin phosphorylation in endothelial cells. HUVECs were cultured for 24 h to allow the consolidation of intercellular junctions and barrier function before incubation with 25 μM Aβ1-42 or scrambled Aβ1-42 (A). The barrier function was monitored by ECIS for 24 h (impedance measurement were performed at frequency 4000 Hz), after which the monolayer was damaged using a high intensity electrical injury (time 1 s, current 1400 μA). The impedance was measured for a further 24 h to assess cell monolayer and barrier function repair. A representative trace for the impedance within the 72 h of the experiments is shown (top panel) and the statistical analysis of data from 6 and 4 independent experiments (pre-wounding and post-wounding assessments, respectively) is shown in the bottom panel. The statistical significance of the difference was assessed by one-way ANOVA with Tukey post-test (*, $p < 0.05$; **, $p < 0.01$; ***, $p < 0.001$). The localisation of VE-cadherin following treatment with Aβ1-42 or scrambled control peptide was tested by immunocytochemistry (B). Following fixation with 4% w/v paraformaldehyde, VE-cadherin localisation was assessed by antibody staining (plus FITC-labelled secondary) and confocal imaging. VE-cadherin localisation at cell-cell junctions (magnified panel) was quantified by image analysis with FIJI software and the statistical significance of the difference was assessed (Mann Whitney non-parametric test; *, $p < 0.05$; **, $p < 0.01$; ***, $p < 0.001$; $n = 4$). Western blotting results show that the treatment of HUVECs with Aβ1-42 increases the phosphorylation levels of VE-cadherin^{Y658} (C). Densitometry analysis of the results is expressed as ratio of phospho-VE-cadherin staining over total VE-cadherin staining (FIJI software). The statistical analysis was performed by Mann Whitney non-parametric test (*, $p < 0.05$; **, $p < 0.01$; ***, $p < 0.001$; $n = 4$).

damage. Although there is no existing consensus on the source of oxidative injury in endothelial cells exposed to amyloid peptide beta [58,59], the role of oxidative stress in the damage of the blood brain barrier and the progression of AD is well-established [60,61]. In this study, we identify NOX1 as the source of superoxide anion in endothelial cells exposed to amyloid peptide β. Superoxide anion is central to the chemistry of ROS, as it can directly modify biological molecules including proteins, nucleic acids and lipids, it can form highly reactive molecules such as peroxynitrite or hydroxyl radical, or it can be transformed hydrogen peroxide by superoxide dismutases [62]. Using pharmacological and genetic manipulations of endothelial cells combined with EPR detection of superoxide anions, we identified NOX1 as the main source of ROS in endothelial cells exposed to amyloid peptide β. The use of the EPR approach is particularly powerful as it allows the quantification of superoxide anion generation rates without the risk of artefacts [63]. NOX1 is indeed an important member of the NOX family with significant expression and physiological function in endothelial cells [64]. Interestingly a previous study on human endothelial cells by Carrano and colleagues reported a redox-dependent mechanism for the impairment of barrier function by amyloid peptide β [25]. Differently to our results, the above study identified NOX2 as the key mediator of the effect of the amyloid peptide β and the authors described the effect was on endothelial tight junctions (TJs). This discrepancy is likely to depend on the differential experimental approach utilised. Carrano and colleagues used Amplex Red for the detection of ROS (which is sensitive mainly to hydrogen peroxide) while we used EPR with a hydroxylamine-based probe (which selectively measures oxygen radicals such as superoxide anions). In addition, Carrano and colleagues

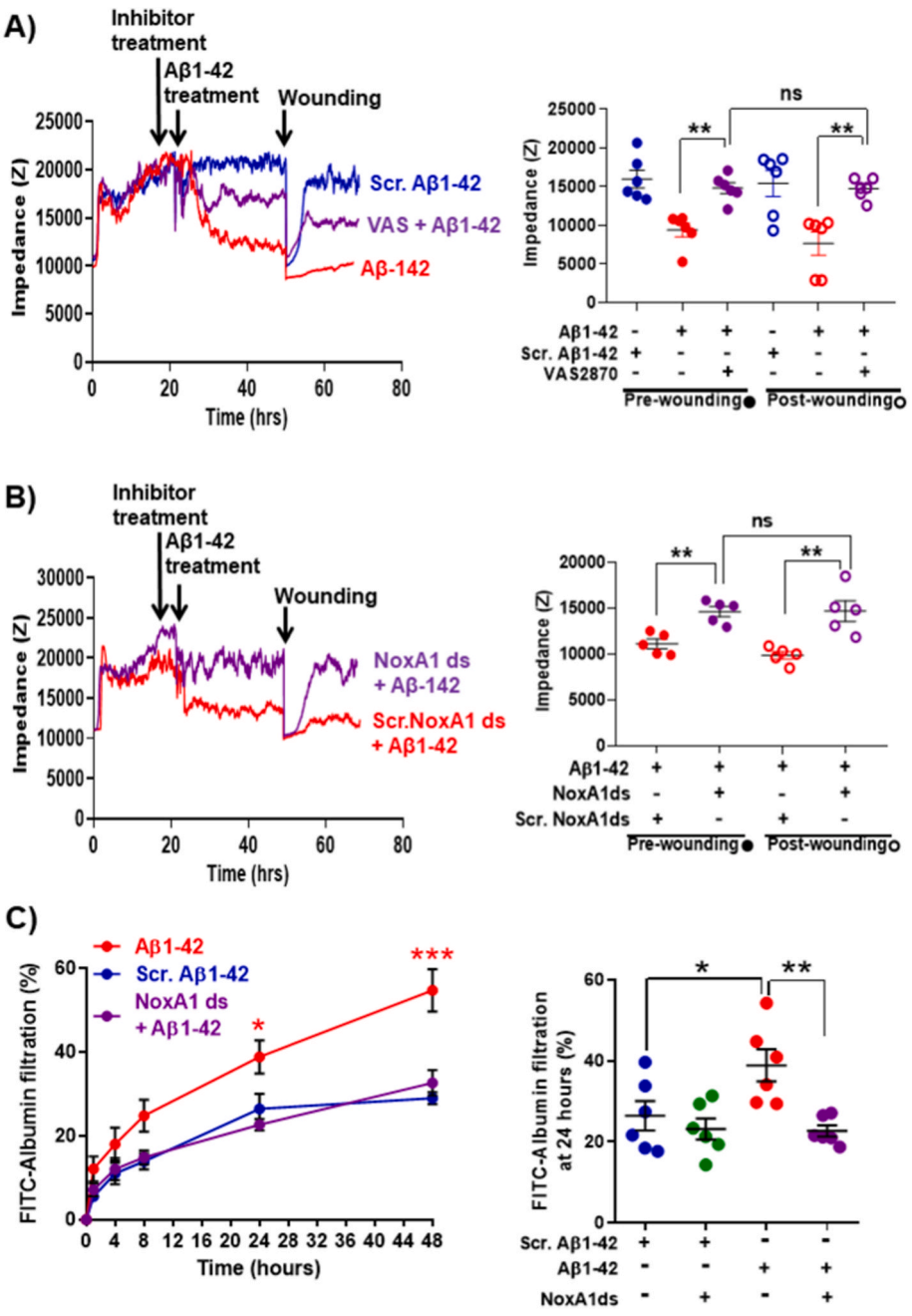

Fig. 7. NOX1 is responsible for the Aβ1-42-dependent impairment of endothelial cell barrier function. The impairment of HUVEC barrier function by 25 μM Aβ1-42 before and after injury was compared to scrambled control peptide in the presence of the pan NOX inhibitor VAS2870 (10 μM, A) and the NOX1-selective inhibitory peptide NoxA1ds (10 μM, B). Scrambled Aβ1-42 (scr. Aβ1-42) was used as negative control. Representative traces for the 72 h-long experiments are shown on the left, while the statistical analysis is shown on the right. The statistical significance of the difference was assessed by one-way ANOVA with Tukey post-test (*, $p < 0.05$; **, $p < 0.01$; ***, $p < 0.001$; $n = 5$ for both A and B). The effect of Aβ1-42 on HUVEC barrier function was analysed using a FITC-albumin permeability assay (C). The treatment with 25 μM Aβ1-42 was monitored for 48 h. Where indicated NOX1-selective inhibitory peptide NoxA1ds was added (10 μM). The time course is shown on the left, while the scatter plot of the data at 24 h is shown on the right. The statistical analysis of the time course was performed by two-way ANOVA with Bonferroni post-test to determine at which time point the monolayer permeability was statistically different from the control condition (i.e. scr. Aβ1-42). The data at 24 h were analysed by one-way ANOVA with Tukey post-test. In both cases, $n = 6$ (*, $p < 0.05$; **, $p < 0.01$; ***, $p < 0.001$).

focused on the effect of amyloid peptide β on the expression of TJ proteins (e.g. claudins, occludins and ZO1), whereas we described endothelial barrier changes occurring by ECIS or FITC-albumin filtration [65]. Overall, our results and the study from Carrano and colleagues are likely to describe two different phenomena contributing in parallel to BBB alterations *in vivo* and in AD patients.

Importantly, although the signalling intermediates remains to be identified, we show that the generation of superoxide anion by NOX1 is absolutely essential for the impairment of endothelial cell barrier function. Because of the increasingly understood heterogeneity of endothelial cell types throughout the human body [66], we confirmed these findings in primary microvascular endothelial cells from human brain. Overall, our data describe a novel molecular mechanism linking amyloid peptide β with a loss of junctional stability and an impairment of barrier function of endothelial cells. Considering the central role of NOX1 in the deleterious effect of amyloid peptide β on the barrier function of endothelial cells *in vitro*, upon confirmation of our findings *in vivo* and in AD patients, NOX1-selective inhibitors may become important candidates for the development of novel drugs able to protect the cerebrovascular integrity of AD patients. By protecting the cerebrovascular function, NOX1 inhibitors may be able to control or slow down the progression of the neurodegeneration in AD patients.

Author contribution statement

AT and NW performed experiments and part of the data analysis for this manuscript. CK and HS performed and analysed the proteomics experiments. HS proofread the manuscript. GP designed the project, planned the experiments, and wrote the manuscript.

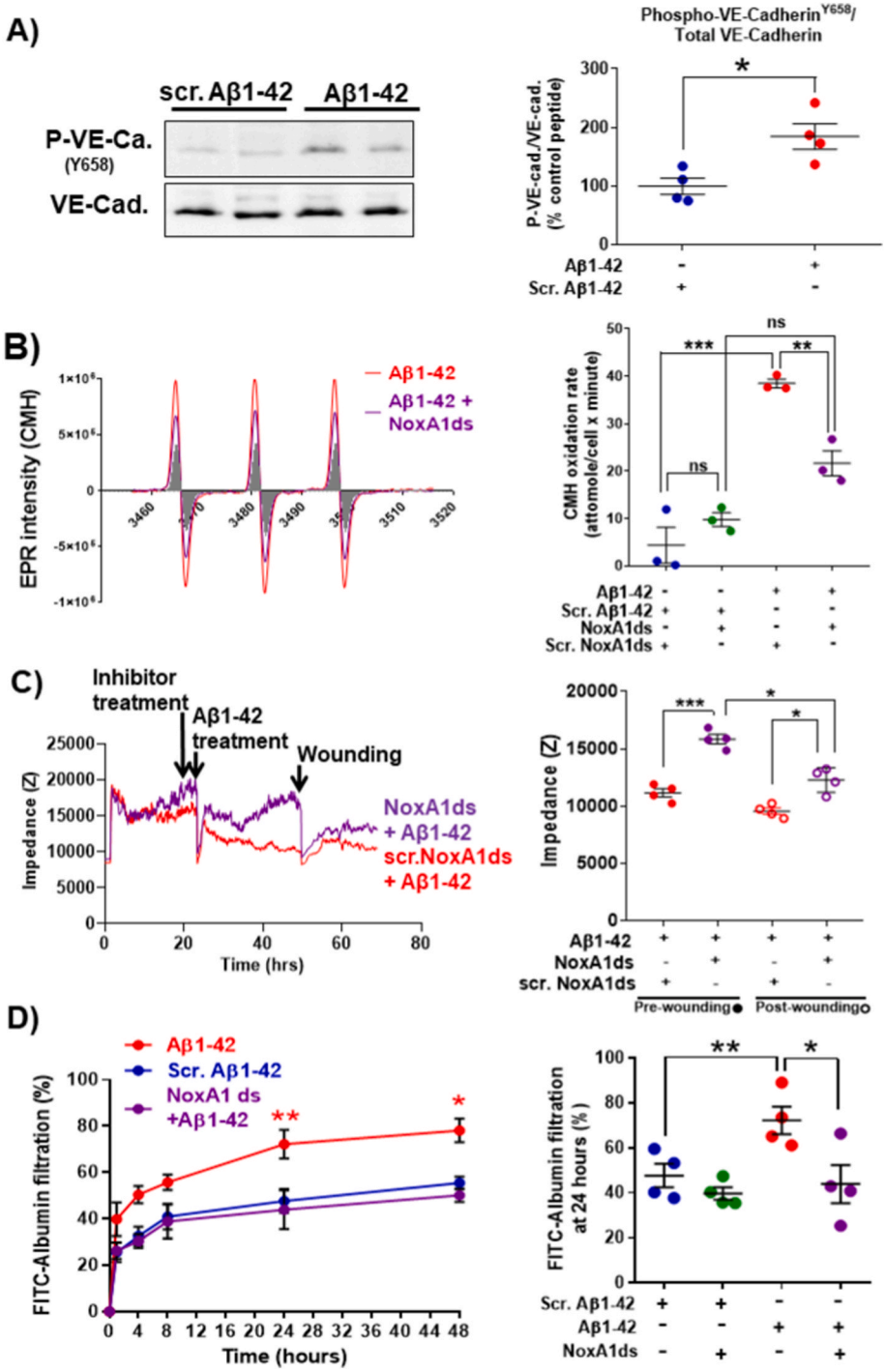

Fig. 8. NOX1 cause oxidative stress and barrier function loss in primary human brain microvascular endothelial cells (hBMEC) treated with Aβ1-42. Western blotting results show that the treatment of hBMECs with Aβ1-42 increases the phosphorylation levels of VE-cadherin^{Y658} (A). Densitometry analysis of the results is expressed as ratio of phospho-VE-cadherin staining over total VE-cadherin staining (FIJI software). The statistical analysis was performed by Mann Whitney non-parametric test (*, $p < 0.05$; **, $p < 0.01$; ***, $p < 0.001$; $n = 4$). CMH-based EPR was utilised for the detection of oxygen radicals generated by hBMECs following a 4 hour treatment with 25 μM Aβ1-42 or scrambled control peptide (B). hBMECs were pre-treated with 10 μM NoxA1ds (or scrambled NoxA1ds peptide). A representative EPR is shown is on the left, while Statistical analysis performed by one-way ANOVA with Turkey test for multiple comparisons is shown on the right (*, $p < 0.05$; **, $p < 0.01$; ***, $p < 0.001$; $n = 3$). The effect of Aβ1-42 on hBMEC barrier function was analysed by ECIS (C). ECIS measurements at 4000 Hz frequency show the endothelial cell barrier function integrity before after electrical injury (time 1 s, current 1400 μA). The loss of junctional integrity before and after injury is corrected by pre-incubation with 10 μM NoxA1ds (versus scrambled NoxA1ds peptide). Representative traces for the 72 h-long experiments are shown on the left, while the statistical analysis is shown on the right. The statistical significance of the difference was assessed by one-way ANOVA with Tukey post-test (*, $p < 0.05$; **, $p < 0.01$; ***, $p < 0.001$; $n = 4$). The effect of Aβ1-42 on hBMEC barrier function was analysed using a FITC-albumin permeability assay (D). The treatment with 25 μM Aβ1-42 was monitored for 48 h. Where indicated NOX1-selective inhibitory peptide NoxA1ds was added (10 μM). The time course is shown on the left, whilst the scatter plot of the data at 24 h is shown on the right. The statistical analysis of the time course was performed by two-way ANOVA with Bonferroni post-test to determine at which time point was the monolayer permeability statistically different from the control (i.e. scr. Aβ1-42). The data at 24 h were analysed by one-way ANOVA with Tukey post-test. In both cases, $n = 4$ (*, $p < 0.05$; **, $p < 0.01$; ***, $p < 0.001$).

Data availability statement

Data in this article will be shared upon reasonable requests to the corresponding author by email.

Declaration of competing interest

The authors declare no conflict of interest.

Acknowledgements

The authors would like to acknowledge the Alzheimer Research UK (ARUK-PG2017A-3), the Werner Otto Foundation (#3/97) and the European Research Council (grant agreement 101025074) for the financial support. The authors would also like to thank Dr Dina Vara for her help with the setting up of the EPR experiments, the Animal facility of the University of Exeter for support with animal experiments, the Histology Unit of the Department of Neurosciences, Physiology and Pharmacology of the University of Bristol for the support of histology experiments, and Dr Antonio Virgilio Failla of the UKE Microscopy Imaging Facility for his assistance with the microscopy experiments.

Appendix A. Supplementary data

Supplementary data to this article can be found online at https://doi.org/10.1016/j.redox.2022.102287.

References

[1] F.J. Wolters, M.A. Ikram, Epidemiology of dementia: the burden on society, the challenges for research, Methods Mol. Biol. 1750 (2018) 3–14, https://doi.org/10.1007/978-1-4939-7704-8_1.

[2] W.W. Barker, et al., Relative frequencies of Alzheimer disease, Lewy body, vascular and frontotemporal dementia, and hippocampal sclerosis in the State of Florida Brain Bank, Alzheimer Dis. Assoc. Disord. 16 (2002) 203–212, https://doi.org/10.1097/00002093-200210000-00001.

[3] H. Hippius, G. Neundorfer, The discovery of Alzheimer's disease, Dialogues Clin. Neurosci. 5 (2003) 101–108.

[4] T. Ozben, S. Ozben, Neuro-inflammation and anti-inflammatory treatment options for Alzheimer's disease, Clin. Biochem. 72 (2019) 87–89, https://doi.org/10.1016/j.clinbiochem.2019.04.001.

[5] B.P. Austin, et al., Effects of hypoperfusion in Alzheimer's disease, J. Alzheimers Dis. 26 (Suppl 3) (2011) 123–133, https://doi.org/10.3233/JAD-2011-0010.

[6] T. Thomas, S. Miners, S. Love, Post-mortem assessment of hypoperfusion of cerebral cortex in Alzheimer's disease and vascular dementia, Brain 138 (2015) 1059–1069, https://doi.org/10.1093/brain/awv025.

[7] G. Zuliani, et al., Markers of endothelial dysfunction in older subjects with late onset Alzheimer's disease or vascular dementia, J. Neurol. Sci. 272 (2008) 164–170, https://doi.org/10.1016/j.jns.2008.05.020.

[8] A. Christov, J. Ottman, L. Hamdheydari, P. Grammas, Structural changes in Alzheimer's disease brain microvessels, Curr. Alzheimer Res. 5 (2008) 392–395.

[9] E. Farkas, P.G. Luiten, Cerebral microvascular pathology in aging and Alzheimer's disease, Prog. Neurobiol. 64 (2001) 575–611.

[10] T.L. Bailey, C.B. Rivara, A.B. Rocher, P.R. Hof, The nature and effects of cortical microvascular pathology in aging and Alzheimer's disease, Neurol. Res. 26 (2004) 573–578, https://doi.org/10.1179/016164104225016272.

[11] L. Ostergaard, et al., The capillary dysfunction hypothesis of Alzheimer's disease, Neurobiol. Aging 34 (2013) 1018–1031, https://doi.org/10.1016/j.neurobiolaging.2012.09.011.

[12] S. Ahtiluoto, et al., Diabetes, Alzheimer disease, and vascular dementia: a population-based neuropathologic study, Neurology 75 (2010) 1195–1202, https://doi.org/10.1212/WNL.0b013e3181f4d7f8.

[13] A. Viswanathan, W.A. Rocca, C. Tzourio, Vascular risk factors and dementia: how to move forward? Neurology 72 (2009) 368–374, https://doi.org/10.1212/01.wnl.0000341271.90478.8e.

[14] B. Borroni, et al., Microvascular damage and platelet abnormalities in early Alzheimer's disease, J. Neurol. Sci. 203–204 (2002) 189–193.

[15] C.A. Szekely, P.P. Zandi, Non-steroidal anti-inflammatory drugs and Alzheimer's disease: the epidemiological evidence, CNS Neurol. Disord. - Drug Targets 9 (2010) 132–139.

[16] L. Thirumangalakudi, P.G. Samany, A. Owoso, B. Wiskar, P. Grammas, Angiogenic proteins are expressed by brain blood vessels in Alzheimer's disease, J. Alzheim. Dis. : JAD 10 (2006) 111–118.

[17] X. Yin, J. Wright, T. Wall, P. Grammas, Brain endothelial cells synthesize neurotoxic thrombin in Alzheimer's disease, Am. J. Pathol. 176 (2010) 1600–1606, https://doi.org/10.2353/ajpath.2010.090406.

[18] P. Grammas, Neurovascular dysfunction, inflammation and endothelial activation: implications for the pathogenesis of Alzheimer's disease, J. Neuroinflammation 8 (2011) 26, https://doi.org/10.1186/1742-2094-8-26.

[19] D. Tripathy, et al., Thrombin, a mediator of cerebrovascular inflammation in AD and hypoxia, Front. Aging Neurosci. 5 (2013) 19, https://doi.org/10.3389/fnagi.2013.00019.

[20] E. Cuevas, et al., Amyloid Beta 25-35 induces blood-brain barrier disruption in vitro, Metab. Brain Dis. 34 (2019) 1365–1374, https://doi.org/10.1007/s11011-019-00447-8.

[21] F. Lamoke, et al., Amyloid beta peptide-induced inhibition of endothelial nitric oxide production involves oxidative stress-mediated constitutive eNOS/HSP90 interaction and disruption of agonist-mediated Akt activation, J. Neuroinflammation 12 (2015) 84, https://doi.org/10.1186/s12974-015-0304-x.

[22] C. Grochowski, J. Litak, P. Kamieniak, R. Maciejewski, Oxidative stress in cerebral small vessel disease. Role of reactive species, Free Radic. Res. 52 (2018) 1–13, https://doi.org/10.1080/10715762.2017.1402304.

[23] T.M. De Silva, A.A. Miller, Cerebral small vessel disease: targeting oxidative stress as a novel therapeutic strategy? Front. Pharmacol. 7 (2016) 61, https://doi.org/10.3389/fphar.2016.00061.

[24] C. Carvalho, P.I. Moreira, Oxidative stress: a major player in cerebrovascular alterations associated to neurodegenerative events, Front. Physiol. 9 (2018) 806, https://doi.org/10.3389/fphys.2018.00806.

[25] A. Carrano, et al., Amyloid Beta induces oxidative stress-mediated blood-brain barrier changes in capillary amyloid angiopathy, Antioxidants Redox Signal. 15 (2011) 1167–1178, https://doi.org/10.1089/ars.2011.3895.

[26] M.D. Potter, S. Barbero, D.A. Cheresh, Tyrosine phosphorylation of VE-cadherin prevents binding of p120- and beta-catenin and maintains the cellular mesenchymal state, J. Biol. Chem. 280 (2005) 31906–31912, https://doi.org/10.1074/jbc.M505568200.

[27] C. Jean, et al., Inhibition of endothelial FAK activity prevents tumor metastasis by enhancing barrier function, J. Cell Biol. 204 (2014) 247–263, https://doi.org/10.1083/jcb.201307067.

[28] S. Oddo, et al., Triple-transgenic model of Alzheimer's disease with plaques and tangles: intracellular Abeta and synaptic dysfunction, Neuron 39 (2003) 409–421, https://doi.org/10.1016/s0896-6273(03)00434-3.

[29] G.J. Gage, D.R. Kipke, W. Shain, Whole animal perfusion fixation for rodents, JoVE (2012), https://doi.org/10.3791/3564.

[30] J. Schindelin, et al., Fiji: an open-source platform for biological-image analysis, Nat. Methods 9 (2012) 676–682, https://doi.org/10.1038/nmeth.2019.

[31] A. Tarafdar, E. Dobbin, P. Corrigan, R. Freeburn, H. Wheadon, Canonical Wnt signaling promotes early hematopoietic progenitor formation and erythroid specification during embryonic stem cell differentiation, PLoS One 8 (2013), e81030, https://doi.org/10.1371/journal.pone.0081030.

[32] D. Vara, et al., Direct activation of NADPH oxidase 2 by 2-deoxyribose-1-phosphate triggers nuclear factor kappa B-dependent angiogenesis, Antioxidants Redox Signal. 28 (2018) 110–130, https://doi.org/10.1089/ars.2016.6869.

[33] D. Vara, E. Cifuentes-Pagano, P.J. Pagano, G. Pula, A novel combinatorial technique for simultaneous quantification of oxygen radicals and aggregation reveals unexpected redox patterns in the activation of platelets by different physiopathological stimuli, Haematologica 104 (2019) 1879–1891, https://doi.org/10.3324/haematol.2018.208819.

[34] C. Tiruppathi, A.B. Malik, P.J. Del Vecchio, C.R. Keese, I. Giaever, Electrical method for detection of endothelial cell shape change in real time: assessment of endothelial barrier function, Proc. Natl. Acad. Sci. U. S. A. 89 (1992) 7919–7923, https://doi.org/10.1073/pnas.89.17.7919.

[35] S.M. Greenberg, et al., Cerebral amyloid angiopathy and Alzheimer disease - one peptide, two pathways, Nat. Rev. Neurol. 16 (2020) 30–42, https://doi.org/10.1038/s41582-019-0281-2.

[36] H. ten Freyhaus, et al., Novel Nox inhibitor VAS2870 attenuates PDGF-dependent smooth muscle cell chemotaxis, but not proliferation, Cardiovasc. Res. 71 (2006) 331–341, https://doi.org/10.1016/j.cardiores.2006.01.022.

[37] D.J. Ranayhossaini, et al., Selective recapitulation of conserved and nonconserved regions of putative NOXA1 protein activation domain confers isoform-specific inhibition of Nox1 oxidase and attenuation of endothelial cell migration, J. Biol. Chem. 288 (2013) 36437–36450, https://doi.org/10.1074/jbc.M113.521344.

[38] G.A. Knock, NADPH oxidase in the vasculature: expression, regulation and signalling pathways; role in normal cardiovascular physiology and its dysregulation in hypertension, Free Radic. Biol. Med. 145 (2019) 385–427, https://doi.org/10.1016/j.freeradbiomed.2019.09.029.

[39] N. Bien-Ly, et al., Lack of widespread BBB disruption in alzheimer's disease models: focus on therapeutic antibodies, Neuron 88 (2015) 289–297, https://doi.org/10.1016/j.neuron.2015.09.036.

[40] R.A. Corriveau, et al., The science of vascular contributions to cognitive impairment and dementia (VCID): a framework for advancing research priorities in the cerebrovascular biology of cognitive decline, Cell. Mol. Neurobiol. 36 (2016) 281–288, https://doi.org/10.1007/s10571-016-0334-7.

[41] C. Iadecola, R.F. Gottesman, Cerebrovascular alterations in alzheimer disease, Circ. Res. 123 (2018) 406–408, https://doi.org/10.1161/CIRCRESAHA.118.313400.

[42] M.D. Sweeney, et al., Vascular dysfunction-The disregarded partner of Alzheimer's disease, Alzheimers Dement. 15 (2019) 158–167, https://doi.org/10.1016/j.jalz.2018.07.222.

[43] S.M. Greenberg, A. Charidimou, Diagnosis of cerebral amyloid angiopathy: evolution of the boston criteria, Stroke 49 (2018) 491–497, https://doi.org/10.1161/STROKEAHA.117.016990.

[44] W.D. Brenowitz, P.T. Nelson, L.M. Besser, K.B. Heller, W.A. Kukull, Cerebral amyloid angiopathy and its co-occurrence with Alzheimer's disease and other cerebrovascular neuropathologic changes, Neurobiol. Aging 36 (2015) 2702–2708, https://doi.org/10.1016/j.neurobiolaging.2015.06.028.

[45] M. Cortes-Canteli, C. Iadecola, Alzheimer's disease and vascular aging: JACC focus seminar, J. Am. Coll. Cardiol. 75 (2020) 942–951, https://doi.org/10.1016/j.jacc.2019.10.062.

[46] D.R. Riddle, W.E. Sonntag, R.J. Lichtenwalner, Microvascular plasticity in aging, Ageing Res. Rev. 2 (2003) 149–168, https://doi.org/10.1016/s1568-1637(02)00064-8.

[47] M.R. Azarpazhooh, et al., Concomitant vascular and neurodegenerative pathologies double the risk of dementia, Alzheimers Dement. 14 (2018) 148–156, https://doi.org/10.1016/j.jalz.2017.07.755.

[48] J.L. Chou, et al., Early dysregulation of the mitochondrial proteome in a mouse model of Alzheimer's disease, J. Proteonomics 74 (2011) 466–479, https://doi.org/10.1016/j.jprot.2010.12.012.

[49] H. Yu, et al., Mitochondrial molecular abnormalities revealed by proteomic analysis of hippocampal organelles of mice triple transgenic for alzheimer disease, Front. Mol. Neurosci. 11 (2018) 74, https://doi.org/10.3389/fnmol.2018.00074.

[50] E. Pauls, et al., Identification and drug-induced reversion of molecular signatures of Alzheimer's disease onset and progression in App(NL-G-F), App(NL-F), and 3xTg-AD mouse models, Genome Med. 13 (2021) 168, https://doi.org/10.1186/s13073-021-00983-y.

[51] X. Zhang, W. Liu, Y. Cao, W. Tan, Hippocampus proteomics and brain lipidomics reveal network dysfunction and lipid molecular abnormalities in APP/PS1 mouse model of alzheimer's disease, J. Proteome Res. 19 (2020) 3427–3437, https://doi.org/10.1021/acs.jproteome.0c00255.

[52] M.K. Elder, et al., Age-dependent shift in the de novo proteome accompanies pathogenesis in an Alzheimer's disease mouse model, Commun. Biol. 4 (2021) 823, https://doi.org/10.1038/s42003-021-02324-6.

[53] S.J.F. van der Spek, et al., Age-dependent hippocampal proteomics in the APP/PS1 alzheimer mouse model: a comparative analysis with classical SWATH/DIA and directDIA approaches, Cells 10 (2021), https://doi.org/10.3390/cells10071588.
[54] H. Oakley, et al., Intraneuronal beta-amyloid aggregates, neurodegeneration, and neuron loss in transgenic mice with five familial Alzheimer's disease mutations: potential factors in amyloid plaque formation, J. Neurosci. 26 (2006) 10129–10140, https://doi.org/10.1523/JNEUROSCI.1202-06.2006.
[55] B. Gurel, et al., Proteomics analysis of CA1 region of the Hippocampus in pre-, progression and pathological stages in a mouse model of the alzheimer's disease, Curr. Alzheimer Res. 16 (2019) 613–621, https://doi.org/10.2174/1567205016666190730155926.
[56] M.G. Lampugnani, et al., The molecular organization of endothelial cell to cell junctions: differential association of plakoglobin, beta-catenin, and alpha-catenin with vascular endothelial cadherin (VE-cadherin), J. Cell Biol. 129 (1995) 203–217, https://doi.org/10.1083/jcb.129.1.203.
[57] K. Hatanaka, M. Simons, M. Murakami, Phosphorylation of VE-cadherin controls endothelial phenotypes via p120-catenin coupling and Rac1 activation, Am. J. Physiol. Heart Circ. Physiol. 300 (2011) H162–H172, https://doi.org/10.1152/ajpheart.00650.2010.
[58] L. Park, et al., Scavenger receptor CD36 is essential for the cerebrovascular oxidative stress and neurovascular dysfunction induced by amyloid-beta, Proc. Natl. Acad. Sci. U. S. A. 108 (2011) 5063–5068, https://doi.org/10.1073/pnas.1015413108.
[59] S. Askarova, X. Yang, W. Sheng, G.Y. Sun, J.C. Lee, Role of Abeta-receptor for advanced glycation endproducts interaction in oxidative stress and cytosolic phospholipase A(2) activation in astrocytes and cerebral endothelial cells, Neuroscience 199 (2011) 375–385, https://doi.org/10.1016/j.neuroscience.2011.09.038.
[60] G. Aliev, et al., Oxidative stress mediated mitochondrial and vascular lesions as markers in the pathogenesis of Alzheimer disease, Curr. Med. Chem. 21 (2014) 2208–2217, https://doi.org/10.2174/0929867321666131227161303.
[61] A.M. Enciu, M. Gherghiceanu, B.O. Popescu, Triggers and effectors of oxidative stress at blood-brain barrier level: relevance for brain ageing and neurodegeneration, 2013, Oxid. Med. Cell. Longev. (2013), 297512, https://doi.org/10.1155/2013/297512.
[62] T.J. Costa, et al., The homeostatic role of hydrogen peroxide, superoxide anion and nitric oxide in the vasculature, Free Radic. Biol. Med. 162 (2021) 615–635, https://doi.org/10.1016/j.freeradbiomed.2020.11.021.
[63] S. Dikalov, M. Skatchkov, B. Fink, E. Bassenge, Quantification of superoxide radicals and peroxynitrite in vascular cells using oxidation of sterically hindered hydroxylamines and electron spin resonance, Nitric Oxide 1 (1997) 423–431, https://doi.org/10.1006/niox.1997.0139.
[64] K. Wingler, et al., NOX1, 2, 4, 5: counting out oxidative stress, Br. J. Pharmacol. 164 (2011) 866–883, https://doi.org/10.1111/j.1476-5381.2011.01249.x.
[65] B. Srinivasan, et al., TEER measurement techniques for in vitro barrier model systems, J. Lab. Autom. 20 (2015) 107–126, https://doi.org/10.1177/2211068214561025.
[66] J.K. Hennigs, C. Matuszcak, M. Trepel, J. Korbelin, Vascular endothelial cells: heterogeneity and targeting approaches, Cells 10 (2021), https://doi.org/10.3390/cells10102712.